



HAL
open science

An adaptive finite element method for viscoplastic flows in a square pipe with stick-slip at the wall

Nicolas Roquet, Pierre Saramito

► **To cite this version:**

Nicolas Roquet, Pierre Saramito. An adaptive finite element method for viscoplastic flows in a square pipe with stick-slip at the wall. 2007. hal-00133116v2

HAL Id: hal-00133116

<https://hal.science/hal-00133116v2>

Preprint submitted on 20 Sep 2007 (v2), last revised 21 Sep 2007 (v3)

HAL is a multi-disciplinary open access archive for the deposit and dissemination of scientific research documents, whether they are published or not. The documents may come from teaching and research institutions in France or abroad, or from public or private research centers.

L'archive ouverte pluridisciplinaire **HAL**, est destinée au dépôt et à la diffusion de documents scientifiques de niveau recherche, publiés ou non, émanant des établissements d'enseignement et de recherche français ou étrangers, des laboratoires publics ou privés.

An adaptive finite element method for viscoplastic flows in a square pipe with stick-slip at the wall

Nicolas Roquet ^a

^a*LCPC – Centre de Nantes, route de Bouaye, BP 4129, 44341 Bouguenais cedex, France*

Pierre Saramito ^b

^b*CNRS – LJK, B.P. 53, 38041 Grenoble cedex 9, France (corresponding author)*

Abstract – This paper is the third of a collection of three papers devoted to the numerical resolution of non-linear yield stress phenomena by using a new mixed anisotropic auto-adaptive finite element method. The first paper (Saramito & Roquet, 2001) revisited the classical fully developed Poiseuille flow of a Bingham yield stress fluid in a straight pipe with non-circular cross-section. The computation showed the efficiency of the method that was able to compute accurately the yield surfaces that separate the shear region from the central plug and the dead zones. The second paper (Roquet & Saramito, 2004) considered the less classical problem of a Newtonian fluid with slip yield boundary condition at the wall. Numerical computations cover the complete range of the dimensionless number describing the slip yield effect, from a full slip to a full stick flow regime. This paper presents a combination of the two previous non-linear yield stress phenomena: the Poiseuille flow of a Bingham fluid with slip yield boundary condition at the wall. Despite its practical interest, for instance for pipeline flows of yield stress fluids such as concrete and cements, this problem has not been addressed to the best of our knowledge. The case of a pipe with a square cross-section has been investigated in detail. The computations cover the full range of the two main dimensionless numbers and exhibit complex flow patterns: all the different flow regimes are completely identified.

Keywords – viscoplasticity; Bingham fluid; slip at the wall; limit load analysis; variational inequalities; adaptive mesh; mixed finite element methods.

Email addresses: Nicolas.Roquet@lcpc.fr (Nicolas Roquet), Pierre.Saramito@imag.fr (Pierre Saramito).

1. Introduction

The flow of a viscoplastic fluid in a straight pipe with constant section and *with non-slip* condition at the wall as been considered several times in the literature. In the 60's, an extensive mathematical study has been achieved by Mossolov and Miasnikov [1,2,3]. These authors have established impressive results on the existence and shape of rigid zones in the flow. In particular, they were the first to characterize the critical value of the yield stress above which the flow stops. See also Huilgol [4] for a recent application of such this approach to several pipes with symmetric cross-section. Next, Duvaut and Lions [5] clarified the the problem of existence and uniqueness of a solution and renewed the mathematical study by using the powerful tools of variational inequalities. They recovered some properties already established by Mossolov and Miasnikov, and found new interesting properties.

The numerical study of this flow problem was first considered in 1972 by M. Fortin [6]. More recently, the regularized model of Bercovier and Engelman [7] has been used by Taylor and Wilson [8] to study the case of a square section. The augmented Lagrangian algorithm from M. Fortin and Glowinski [9] has been used by Huilgol and Panizza [10] to solve the case of an annulus and of an L-shaped cross-section, with the Bingham rheology. More recently, Huilgol and You [11] have derived the algorithm for two other viscoplastic rheologies (Casson and Herschel-Bulkley).

In 2001, Saramito and Roquet revisited the classical fully developed Poiseuille flow of a Bingham yield stress fluid in pipe [12] with general (non-circular) cross-section. Addressing the case of a square section, they pointed out the lack of precision of the previous numerical computations, that was not able to compute accurately the yield surfaces that separates the shear region from the central plug and the dead zones. They proposed a new mixed anisotropic auto-adaptive finite element method coupled to the augmented Lagrangian algorithm. The mesh refinement is expected to catch accurately the free boundaries of the rigid zones. Based on *a priori* error estimate on adapted meshes, Roquet *et al.* [13] performed the numerical analysis of the method and showed that it converges with an optimal global order of accuracy. Finally, the extension of this approach to more general flows of a Bingham fluid is addressed in [14] were the authors considered the flow around a cylinder.

In practical viscoplastic flow problems such as concrete pumping (see e.g. [15,16]), it appears that a non-slip boundary condition is not a satisfying model. The fluid slips when the tangential strength exceeds a critical value, and, otherwise the fluid sticks at the wall. This critical value may be considered as an intrinsic characteristic of the material: in the following, it will be called the *yield-force* of the fluid. The model defined by Weber [15] describes this yield-force slip phenomenon. It has already been used by for the flow of a Newtonian fluid with the Weber slip law by A. Fortin *et al.* [17] for the sudden contraction geometry and next by Roquet and Saramito [18] for the straight pipe flow with a square cross-section.

The aim of this paper is to extend the technique presented in Saramito and Roquet [12,18] in order to apply it to the flow of a Bingham fluid in a straight pipe with constant section with the Weber slip law at the wall. In section 2, all the governing laws of the flow model are presented, ending with the non-dimensional formulation of the flow of a Bingham fluid with the Weber law in a straight pipe. In the third section, the numerical method is described. The last section presents all the numerical results and the discussion. The role of the two dimensionless numbers associated to the yield parameters of the flow structure are investigated with details. The computations cover the full range of the two main dimensionless numbers and exhibit complex flow patterns: all the different flow regimes are completely identified.

2. Problem statement

The general equations for the flow of a Bingham fluid with the Weber law is given first. Then, it is specialized for the case of a straight pipe with constant cross-section.

2.1. Constitutive equation and conservation laws

Let σ_{tot} denotes the total Cauchy stress tensor:

$$\sigma_{\text{tot}} = -pI + \sigma, \quad (1)$$

where σ denotes its deviatoric part, and p the pressure. In this paper, the fluid is supposed to be viscoplastic, and the relation between σ and $D(\mathbf{u})$ is given by the Bingham model [19,20]:

$$\begin{cases} \sigma = 2\eta D(\mathbf{u}) + \sigma_0 \frac{D(\mathbf{u})}{|D(\mathbf{u})|} & \text{when } D(\mathbf{u}) \neq 0 \\ |\sigma| \leq \sigma_0 & \text{when } D(\mathbf{u}) = 0 \end{cases} \quad (2)$$

here $\sigma_0 \geq 0$ is the yield stress, $\eta > 0$ is the constant viscosity, \mathbf{u} is the velocity field and $D(\mathbf{u}) = (\nabla \mathbf{u} + \nabla \mathbf{u}^T)/2$. For any tensor $\tau = (\tau_{ij})$, the notation $|\tau|$ represents the matrix norm:

$$|\tau| = \left(\frac{\tau : \tau}{2} \right)^{1/2} = \frac{1}{\sqrt{2}} \left(\sum_{i,j} \tau_{ij}^2 \right)^{1/2} \quad (3)$$

The constitutive equation (2) writes equivalently:

$$D(\mathbf{u}) = \begin{cases} \left(1 - \frac{\sigma_0}{|\sigma|} \right) \frac{\sigma}{2\eta} & \text{when } |\sigma| > \sigma_0 \\ 0 & \text{otherwise} \end{cases} \quad (4)$$

The slip boundary condition reads :

$$\mathbf{u}_{\mathbf{t}} = \begin{cases} - \left(1 - \frac{s_0}{|\sigma_{\mathbf{nt}}|} \right) \frac{\sigma_{\mathbf{nt}}}{c_f}, & \text{when } |\sigma_{\mathbf{nt}}| > s_0, \\ 0, & \text{otherwise,} \end{cases} \quad (5)$$

where $s_0 \geq 0$ the slip yield stress and $c_f > 0$ the friction dissipation coefficient. The notations $\mathbf{u}_{\mathbf{t}}$ and $\sigma_{\mathbf{nt}}$ are defined by

$$\begin{aligned} \mathbf{u}_{\mathbf{t}} &= \mathbf{u} - (\mathbf{u} \cdot \mathbf{n}) \mathbf{n}, \\ \sigma_{\mathbf{nt}} &= \sigma \cdot \mathbf{n} - (\sigma_{\mathbf{nn}}) \mathbf{n}, \end{aligned} \quad (6)$$

where $\sigma_{\mathbf{nn}} = (\sigma \cdot \mathbf{n}) \cdot \mathbf{n}$ and \mathbf{n} is the unit outward normal vector. For any vector field \mathbf{v} , the notation $|\cdot|$ represents the vector norm $|\mathbf{v}| = (\mathbf{v} \cdot \mathbf{v})^{1/2}$. Notice that the vector field $\sigma_{\mathbf{nt}}$ is tangent to the boundary and that $\sigma_{\mathbf{nn}}$ is a scalar field defined on the boundary. Observe the analogy of structure between the slip law (5) and the Bingham constitutive equation (4). The slip relation can be also written as:

$$\begin{cases} \sigma_{\mathbf{nt}} = -c_f \mathbf{u}_{\mathbf{t}} - s_0 \frac{\mathbf{u}_{\mathbf{t}}}{|\mathbf{u}_{\mathbf{t}}|}, & \text{when } |\mathbf{u}_{\mathbf{t}}| \neq 0, \\ |\sigma_{\mathbf{nt}}| \leq s_0, & \text{when } |\mathbf{u}_{\mathbf{t}}| = 0. \end{cases} \quad (7)$$

Again, observe the analogy between (7) and (2). The boundary condition is complemented by a condition expressing that the fluid does not cross the boundary:

$$\mathbf{u} \cdot \mathbf{n} = 0. \quad (8)$$

We remark that for $s_0 = 0$, one obtains the classical linear slip boundary condition: the fluid slips for any non-vanishing shear stress $\sigma_{\mathbf{nt}}$. For $s_0 > 0$, boundary parts where the fluid sticks can be observed. As s_0 becomes larger, these stick regions develop. This simple law can be extended, as mentioned by Fortin *et al.* [17] or Ionescu and Vernescu [21]. In the context of solid mechanics and contact problems, Coulomb type friction has been studied by many authors. Refer e.g. to Haslinger *et al.* [22, p. 377] for the numerical analysis and to Kikuchi and Oden [23] for the finite element approximation. In this case, the slip yield stress s_0 is no more a constant, and should be replaced by a quantity s that depends upon the pressure at the boundary: $s = c_0 |\sigma_{\mathbf{nn}}|$. Nevertheless, previous works do not study the stick-slip transition. In this paper, since our purpose is to study a new numerical algorithm for the stick-slip transition capturing, we suppose that the slip yield stress is a constant. The system of equations is closed by conservation laws. The conservation of momentum is:

$$\rho \left(\frac{\partial \mathbf{u}}{\partial t} + \mathbf{u} \cdot \nabla \mathbf{u} \right) - \mathbf{div} \sigma + \nabla p = 0, \quad (9)$$

where ρ is the constant density. Since the fluid is supposed to be incompressible, the mass conservation leads to:

$$\mathbf{div} \mathbf{u} = 0. \quad (10)$$

2.2. The pipe flow problem

We consider the fully developed flow in a prismatic tube (see Fig 1). Let (Oz) be the axis of the tube and (Oxy) the plane of the bounded cross-section $\Omega \subset \mathbb{R}^2$. The pressure gradient is written as $\nabla p = (0, 0, -f)$ in Ω , where $f > 0$ is the constant applied force density.

The velocity is written as $\mathbf{u} = (0, 0, u)$, where the third component u along the (Oz) axis depends only upon x and y , and is independent of t and z . The problem can be written as a two-dimensional one, and the stress tensor σ is equivalent to a two shear stress component vector: $\sigma = (\sigma_{xz}, \sigma_{yz})$. We also use the following notations:

$$\nabla u = \left(\frac{\partial u}{\partial x}, \frac{\partial u}{\partial y} \right) \quad (11)$$

$$\mathbf{div} \sigma = \frac{\partial \sigma_{xz}}{\partial x} + \frac{\partial \sigma_{yz}}{\partial y} \quad (12)$$

$$|\sigma| = (\sigma_{xz}^2 + \sigma_{yz}^2)^{1/2} \quad (13)$$

Finally, the problem of the flow of a Bingham fluid in a pipe with slip at the wall can be summarized as:

(P): find σ and u defined in Ω such that

$$\mathbf{div} \sigma = -f \text{ in } \Omega, \quad (14)$$

$$\max \left(0, 1 - \frac{\sigma_0}{|\sigma|} \right) \sigma - \eta \nabla u = 0 \text{ in } \Omega, \quad (15)$$

$$\max \left(0, 1 - \frac{s_0}{|\sigma \cdot \mathbf{n}|} \right) \sigma \cdot \mathbf{n} + c_f u = 0 \text{ on } \partial\Omega, \quad (16)$$

where \mathbf{n} is the unit outward normal vector on the boundary $\partial\Omega$ of the cross-section Ω . Here (14) expresses the conservation of momentum, (15) the constitutive equation and (16) the slip boundary condition.

Let L be a characteristic length of the cross-section Ω , e.g. the half-length of an edge of a square cross-section. A characteristic velocity is given by $U = L^2 f / \eta$. The Bingham dimensionless number Bi is defined by the ratio of yield stress σ_0 by the representative stress Σ :

$$Bi = \frac{\sigma_0}{L f}. \quad (17)$$

The slip yield dimensionless number S is defined as the ratio of the slip yield stress s_0 to a characteristic stress $\Sigma = \eta U / L = L f$:

$$S = \frac{s_0}{L f}. \quad (18)$$

The friction dimensionless number C_f is defined by

$$C_f = \frac{c_f U}{\Sigma} = \frac{c_f L}{\eta}. \quad (19)$$

The three dimensionless numbers Bi , S and C_f characterize the problem. In order to focus on the non-linear phenomena only, the C_f coefficient is chosen equal to the unity for all numerical experiments. In this paper, we explore the problem related to the variation of both Bi and S . For the kind of flow presented here, the relevant values of the dimensionless numbers Bi and S are expected to be in a finite range, with an upper bound that may depend on the shape of the cross-section. This is due to the existence of critical values of Bi and S above which the non-linear effects do not change the stick-slip transition and the evolution of rigid zones (see for example [12] for Bi only and [18] for S only). One objective of this article is the determination of such critical values.

3. Numerical method

The augmented Lagrangian method, applied to problem (14)-(15), is briefly introduced in this paragraph. Then, the delicate problem of the choice of a finite element approximation is carefully treated.

3.1. Augmented Lagrangian algorithm

Let $H^1(\Omega)$ denote the classical functional Sobolev space [24] and J the convex functional defined for all $v \in H^1(\Omega)$ by

$$J(v) = \frac{\eta}{2} \int_{\Omega} |\nabla v|^2 dx + \frac{c_f}{2} \int_{\partial\Omega} |\gamma v|^2 ds + \sigma_0 \int_{\Omega} |\nabla v| dx + s_0 \int_{\partial\Omega} |\gamma v| ds - \int_{\Omega} f v dx \quad (20)$$

where ds is a measure on $\partial\Omega$ and γ is the trace operator from $H^1(\Omega)$ to $H^{1/2}(\partial\Omega)$, i.e. γv is the restriction $v|_{\partial\Omega}$ of v on $\partial\Omega$.

Using variational inequality methods (see e.g. Glowinski *et al.* [25]) we show that the solution u of problem (P) is the minimum of J on $H^1(\Omega)$:

$$\min_{v \in H^1(\Omega)} J(v). \quad (21)$$

Let us introduce two additional variables:

$$\mathbf{d} = \nabla u \in L^2(\Omega)^2, \quad (22)$$

$$\xi = \gamma u \in H^{1/2}(\partial\Omega). \quad (23)$$

These additional constraints are handled by using two corresponding Lagrangian multipliers. The first one, associated with the constraint (22) coincides with the shear stress vector $\boldsymbol{\sigma} \in L^2(\Omega)^2$ and is still denoted by $\boldsymbol{\sigma}$. The second Lagrangian multiplier $\lambda \in L^2(\partial\Omega)$, associated with the constraint (23), coincides with the shear stress $-\boldsymbol{\sigma} \cdot \mathbf{n}$ at the boundary. The Lagrangian \mathcal{L} is defined for all $(u, \mathbf{d}, \xi) \in H^1(\Omega) \times L^2(\Omega)^2 \times L^2(\partial\Omega)$ and $(\boldsymbol{\sigma}, \lambda) \in L^2(\Omega)^2 \times L^2(\partial\Omega)$ by

$$\mathcal{L}((u, \mathbf{d}, \xi); (\boldsymbol{\sigma}, \lambda)) = \frac{\eta}{2} \int_{\Omega} |\mathbf{d}|^2 dx + \sigma_0 \int_{\Omega} |\mathbf{d}| dx - \int_{\Omega} f u dx + \int_{\Omega} \boldsymbol{\sigma} \cdot (\nabla u - \mathbf{d}) dx \quad (24)$$

$$+ \frac{c_f}{2} \int_{\partial\Omega} |\xi|^2 ds + s_0 \int_{\partial\Omega} |\xi| ds + \int_{\partial\Omega} \lambda (\gamma u - \xi) ds. \quad (25)$$

For all $a > 0$, the augmented Lagrangian

$$\mathcal{L}_a((u, \mathbf{d}, \xi); (\boldsymbol{\sigma}, \lambda)) = \mathcal{L}((u, \mathbf{d}, \xi); (\boldsymbol{\sigma}, \lambda)) + \frac{a}{2} \int_{\Omega} |\mathbf{d} - \nabla u|^2 dx + \frac{a}{2} \int_{\partial\Omega} (\xi - \gamma u)^2 ds \quad (26)$$

is quadratic and positive-definite with respect to u . This implies that, with $(\boldsymbol{\sigma}, \lambda)$ and (\mathbf{d}, ξ) fixed, \mathcal{L}_a can be minimized with respect to u on $H^1(\Omega)$, whereas this operation is in practice impossible for $a = 0$. This transformation proves to be helpful since we can solve the saddle-point problem of \mathcal{L}_a , which coincides with that of \mathcal{L} , by an appropriate algorithm proposed in [9]:

ALGORITHM (Uzawa)

initialization: $n = 0$

Let $(\boldsymbol{\sigma}^0, \lambda^0)$ and (\mathbf{d}^0, ξ^0) be arbitrarily chosen in $L^2(\Omega)^2 \times L^2(\partial\Omega)$.

loop: $n \geq 0$

• **step 1:** Suppose $(\boldsymbol{\sigma}^n, \lambda^n)$ and (\mathbf{d}^n, ξ^n) are known and find $u^{n+1} \in H^1(\Omega)$ such that

$$-a\Delta u^{n+1} = f + \operatorname{div}(\boldsymbol{\sigma}^n - a\mathbf{d}^n) \text{ in } \Omega, \quad (27)$$

$$\frac{\partial u^{n+1}}{\partial n} + u^{n+1} = \mathbf{d}^n \cdot \mathbf{n} + \xi^n - \frac{1}{a}(\lambda^n + \boldsymbol{\sigma}^n \cdot \mathbf{n}) \text{ on } \partial\Omega. \quad (28)$$

• **step 2:** compute explicitly in Ω :

$$\mathbf{d}^{n+1} := \begin{cases} \left(1 - \frac{\sigma_0}{|\boldsymbol{\sigma}^n + a\nabla u^{n+1}|}\right) \frac{\boldsymbol{\sigma}^n + a\nabla u^{n+1}}{\eta + a}, & \text{when } |\boldsymbol{\sigma}^n + a\nabla u^{n+1}| > \sigma_0, \\ 0, & \text{otherwise.} \end{cases} \quad (29)$$

and on $\partial\Omega$:

$$\xi^{n+1} := \begin{cases} \left(1 - \frac{s_0}{|\lambda^n + a\gamma u^{n+1}|}\right) \frac{\lambda^n + a\gamma u^{n+1}}{c_f + a}, & \text{if } |\lambda^n + a\gamma u^{n+1}| > s_0, \\ 0, & \text{otherwise.} \end{cases} \quad (30)$$

• **step 3:** compute explicitly:

$$\boldsymbol{\sigma}^{n+1} := \boldsymbol{\sigma}^n + a (\nabla u^{n+1} - \mathbf{d}^{n+1}) \text{ in } \Omega, \quad (31)$$

$$\lambda^{n+1} := \lambda^n + a (\gamma u^{n+1} - \xi^{n+1}) \text{ on } \partial\Omega. \quad (32)$$

end loop

The advantage of this algorithm is that it transforms the global non-differentiable problem (21) into a family of completely standard problems (27)-(28) and local explicit computations (29)-(30), coordinated via the Lagrange multipliers in (31)-(32). The sequence $(u^n, \mathbf{d}^n, \xi^n, \boldsymbol{\sigma}^n, \lambda^n)$ converges for all $a > 0$ to $(u, \mathbf{d}, \xi, \boldsymbol{\sigma}, \lambda)$ where $u \in H^1(\Omega)$ is the solution to (21) and $\mathbf{d} = \nabla u$, $\xi = u|_{\partial\Omega}$, $\boldsymbol{\sigma}$ is the shear stress and $\lambda = -\boldsymbol{\sigma} \cdot \mathbf{n}$ on $\partial\Omega$.

3.2. Finite element approximation

Let A and B be the two bilinear forms defined by:

$$\begin{aligned} A((u, \mathbf{d}, \xi); (v, \boldsymbol{\delta}, \zeta)) &= (\eta + a) \int_{\Omega} \mathbf{d} \cdot \boldsymbol{\delta} \, dx + (c_f + a) \int_{\partial\Omega} \gamma u \gamma v \, ds \\ &\quad + a \int_{\Omega} (\nabla u \cdot \nabla v - \nabla u \cdot \boldsymbol{\delta} - \mathbf{d} \cdot \nabla v) \, dx + a \int_{\partial\Omega} (\gamma u \gamma v - \gamma u \zeta - \xi \gamma v) \, ds, \quad (33) \\ B((v, \boldsymbol{\delta}, \zeta); (\boldsymbol{\tau}, \mu)) &= \int_{\Omega} \boldsymbol{\tau} \cdot (\nabla v - \boldsymbol{\delta}) \, dx + \int_{\partial\Omega} \mu (\gamma v - \zeta) \, ds. \end{aligned}$$

and j be the following function:

$$j(\boldsymbol{\delta}, \zeta) = \sigma_0 \int_{\Omega} |\boldsymbol{\delta}| \, dx + s_0 \int_{\partial\Omega} |\zeta| \, ds \quad (34)$$

The saddle point of \mathcal{L}_a is characterized as the solution of a problem expressed by the following variational inequalities:

(VI): find $(u, \mathbf{d}, \xi) \in H^1(\Omega) \times L^2(\Omega)^2 \times L^2(\partial\Omega)$ and $(\boldsymbol{\sigma}, \lambda) \in L^2(\Omega)^2 \times L^2(\partial\Omega)$ such that:

$$\begin{aligned} j(\boldsymbol{\delta}, \zeta) - j(\mathbf{d}, \xi) + A((u, \mathbf{d}, \xi); (v, \boldsymbol{\delta}, \zeta)) + B((v, \boldsymbol{\delta}, \zeta); (\boldsymbol{\sigma}, \lambda)) &\geq \int_{\Omega} f v \, dx, \\ B((u, \mathbf{d}, \xi); (\boldsymbol{\tau}, \mu)) &= 0 \end{aligned} \quad (35)$$

for all $(v, \boldsymbol{\delta}, \zeta) \in H^1(\Omega) \times L^2(\Omega)^2 \times L^2(\partial\Omega)$ and $(\boldsymbol{\tau}, \lambda) \in L^2(\Omega)^2 \times L^2(\partial\Omega)$.

Let $V_h \subset H^1(\Omega)$, be a finite dimensional space and let $D_h = \nabla V_h$ and $\Xi_h = \gamma V_h$. The finite dimensional version of the variational inequalities is simply obtained by replacing functional spaces by their finite dimensional counterparts:

(VI)_h: find $(u_h, \mathbf{d}_h, \xi_h) \in V_h \times D_h \times \Xi_h$ and $(\boldsymbol{\sigma}_h, \lambda_h) \in D_h \times \Xi_h$ such that:

$$\begin{aligned} j(\boldsymbol{\delta}, \zeta) - j(\mathbf{d}_h, \xi_h) + A((u_h, \mathbf{d}_h, \xi_h); (v, \boldsymbol{\delta}, \zeta)) + B((v, \boldsymbol{\delta}, \zeta); (\boldsymbol{\sigma}_h, \lambda_h)) &\geq \int_{\Omega} f v \, dx, \\ B((u_h, \mathbf{d}_h, \xi_h); (\boldsymbol{\tau}, \mu)) &= 0 \end{aligned} \quad (36)$$

for all $(v, \boldsymbol{\delta}, \zeta) \in V_h \times D_h \times \Xi_h$ and $(\boldsymbol{\tau}, \lambda) \in D_h \times \Xi_h$. Let \mathcal{T}_h be a finite element mesh made up of triangles and let $\partial\mathcal{T}_h$ denote the corresponding mesh of the boundary $\partial\Omega$, consisting in segments. We define V_h as the space of continuous piecewise polynomials of order $k \geq 1$, relative to \mathcal{T}_h :

$$V_h = \{v \in H^1(\Omega); v|_K \in P_k, \forall K \in \mathcal{T}_h\}. \quad (37)$$

Thus, $D_h = \nabla V_h$ is the set of discontinuous piecewise polynomials of order $k - 1$, relative to \mathcal{T}_h :

$$D_h = \{\boldsymbol{\delta} \in L^2(\Omega)^2; \boldsymbol{\delta}|_K \in (P_{k-1})^2, \forall K \in \mathcal{T}_h\}. \quad (38)$$

Conversely, $Xi_h = \gamma V_h$ is the set of continuous piecewise polynomial functions defined on the mesh boundary $\partial\mathcal{T}_h$

$$\Xi_h = \Lambda_h = \{\mu \in L^2(\partial\Omega) \cap C^0(\partial\Omega); \mu|_S \in P_k, \forall S \in \partial\mathcal{T}_h\}. \quad (39)$$

Numerical experiments presented in this paper use piecewise linear polynomials, i.e. $k = 1$.

3.3. Mesh adaptation

The mesh adaptation procedure has already been described in [12,13,14,18] for a Bingham fluid flow problem and in [18] for a stick-slip transition of a Newtonian fluid flow problem. Thus, only the main steps are presented in this paragraph.

A way to adapt the mesh to the computation of a *governing field* is to equi-distribute its error of interpolation, i.e. to make it constant over all triangles and in all directions. Solving a problem using a mesh adaptation is an iterative process, which involves three main steps:

1. Starting from an initial mesh \mathcal{T}_0 , the problem is solved using the augmented Lagrangian algorithm, yielding a solution $u^{(0)}$ associated with the mesh \mathcal{T}_0 .
2. Let $\varphi^{(0)} = |\nabla u^{(0)}|$ be the governing field. This field emphasizes regions where the solution has high derivatives, so that the mesh generator refines these regions.
3. Starting from the governing field $\varphi^{(0)}$ on the mesh \mathcal{T}_0 , an anisotropic adaptive mesh generator (see Borouchaki *et al.* [26], Hecht [27]) generates a totally new mesh, denoted by \mathcal{T}_1 .

Then, \mathcal{T}_1 is used to solve the problem, and so on, until the solution obtained reaches an accurate localization of the stick-slip transition point. This method is based on the fact that high second derivatives of the velocity develop at the neighborhood of the stick-slip transition point, and thus the mesh generator refines this neighborhood. The singular behavior of the second derivative of the velocity at the neighborhood of the transition point will be analyzed in detail in the next section. The software is based on a finite element library released by the authors [28,29].

In order to reduce the computational cost in the square cross-section, we exploit the symmetries of the solutions with respect to the Ox , Oy and the $x = y$ axis. Thus the domain of computation reduces to a triangle (see Fig. 2). Fig. 3 shows the mesh after 15 adaptation loops and for yield numbers $Bi = 0$ and $S = 0.385$, as defined in (17) and (18). The stick-slip transition point is close to the upper corner $x = y = 1$, and the stick region is small. Observe that the mesh adaptation process is able to capture the stick-slip transition point.

4. Numerical experiments and identification of the flow regimes

4.1. Flow features and terminology

The schematic view of the solution is represented on Fig. 4 and, for convenience, we introduce a specific terminology explained by Fig. 4.a. There are two types of rigid zones: the *dead zones*, located in the corners

of the cross-section, associated with $u = 0$, and the *plug*, in the center of the cross-section, associated with a constant velocity. These rigid zones are separated by a *deforming* zone where the velocity varies gradually. The rigid zones are separated from the deforming zone by two surfaces: the dead zone boundary and the plug boundary. At the boundary of the cross-section, there is a *stick region*, where $u_{\partial\Omega} = 0$ and a *slip region* where the velocity is not zero. Finally, the *transition point* separates the stick and the slip regions.

In this section, the extension of the rigid zones and of the slip region are studied, using lengths shown on Fig. 4.b. Along the diagonal of the cross-section, ξ_b is the distance from the center of the square to the boundary of central plug, and ξ_m is the distance between the center of the square and the boundary of the dead zones. Along an edge of the square cross-section, y_T is half the extension of the slip region, and y_m is the distance between the center of the edge and the boundary of the dead zones.

The case $S = +\infty$, corresponding to a Bingham fluid flow that sticks at the wall, has been already studied in detail in [12] while the case $Bi = 0$, corresponding to a Newtonian fluid that may slip at the wall, has been studied in [18]. Thus, the present paper focuses on the cases where non-linear behaviours occur both inside the flow and at the boundary.

4.2. Flow with a fixed slip condition

When the value of the dimensionless parameter S is fixed, and Bi varies, the evolution of the velocity profiles and the rigid zones can be observed. In the particular case when $S = +\infty$, the fluid sticks at the wall and we know that there exists a particular value $Bi_B > 0$ such that the flow stops when $Bi \geq Bi_B$. This result has been proved for a general tube cross-section Ω in [5] and the value $Bi_B = \frac{2}{2+\sqrt{\pi}}$ has been obtained analytically in [1] for a square cross-section and by a numerical method in [12].

The presence of a slip condition modifies this behaviour: the results depend upon the value of S . There exists a particular value Bi_T such that the flow is a rigid translation motion when $Bi \geq Bi_T$. The translation velocity U_T could be zero in some cases, and then the flow stops.

The value of Bi_T depends upon the dimensionless parameter S . When S is small enough, the flow tends, when Bi increases, to a rigid translation and fully slips at the wall. Conversely, when S is large enough, the flow tends, when Bi increases, to stop.

4.2.1. Convergence to the cessation of flow

In this paragraph, let us fix $S = 0.6$.

First, observe on Fig. 5.a the velocity profiles at the wall versus the y coordinate for various values of Bi . All curves decrease with Bi . Each curve reaches a maximum with an horizontal tangent at the center of the boundary cross-section, associated with $y = 0$. For each $Bi \geq 0$, we observe that there exists a point y_T that separates the slip and the stick region: when $y \geq y_T$ the fluid sticks. Notice that the tangent in $y = y_T$ is not horizontal and thus, the velocity gradient is discontinuous along the boundary of the cross-section.

For each fixed y , the velocity at the wall is a decreasing function of Bi . Fig. 5.b shows the maximal wall velocity $u_{\max, \partial\Omega}$, reached at $y = 0$, as a function of Bi for $S = 0.6$. We observe that when Bi is larger than a critical value, denoted by $Bi_A \approx 0.36$, the velocity at the wall is zero all along the wall: the fluid sticks.

The position y_T of the transition point between the slip and the stick region is represented on Fig. 5.c as a function of Bi . This representation shows that y_T is a decreasing function that vanishes for $Bi = Bi_A$.

We have shown the following properties :

- There exists a value Bi_A such that when $Bi < Bi_A$ the material slips in the central region of the wall and sticks close to the corner. When $Bi > Bi_A$, the fluid fully sticks at the wall.
- The velocity at the wall decreases with Bi at each point of the wall.
- The stick region develops with increasing Bi until the total adhesion at the wall is reached at $Bi = Bi_A$.

We now examine the solution inside the flow domain: let us consider the velocity along the axis and the development of rigid zones.

Fig. 6.a shows the velocity profiles along the horizontal axis $y = 0$ for different values of Bi . We observe decreasing and concave curves that reach a maximum at the center of the flow $x = 0$. The velocity is decreasing with Bi at each position x . Moreover, at the center $x = 0$, the profiles exhibit a plateau that grows with Bi : it is associated with the development of a central plug flow region.

Fig. 6.b shows the velocity profiles along the diagonal axis of symmetry: notice that the material sticks at the wall before the plug reaches the wall. Also observe that in the corners of the square cross-section, i.e. at the vicinity of $\xi = \sqrt{2}$, the velocity vanishes: the material sticks at the wall and develops a dead zone. The size of the dead zone depends upon Bi .

The velocity of the plug region is also the maximum velocity $u_{max;\Omega}$ in the pipe cross-section: it is represented versus Bi on Fig. 7.a. Observe that $u_{max;\Omega}$ is a decreasing function of Bi and that it vanishes for $Bi = Bi_T \approx 0.53$. The value $Bi_T \approx 0.53$ is a critical value when the flow stops. This value $Bi_T \approx 0.53$ is obtained numerically and it coincides with the explicitly known critical value for the cessation of flow associated with adhesion at the wall [12]:

$$Bi_T = \frac{2}{2 + \sqrt{\pi}} \approx 0.5301589$$

This observation is consistent with the fact that the material sticks to the wall when $Bi \in]Bi_A; Bi_T[$.

Let us now observe the flow rate as a function of Bi , on Fig. 7.b. The curve first linearly decreases and then smoothly tends to 0, corresponding to the blocking configuration at $Bi = Bi_T$.

Fig. 8 represents the development of rigid zones for $S = 0.6$ versus Bi and the associated adapted meshes. The development of rigid zones for $S = 0.6$ is similar to the case when the material sticks at the wall, that was previously presented in a separate work [12]: a central plug zone, convex and quasi-circular, develops. Its area increases with Bi and its boundary flattens when approaching the wall. Simultaneously, concave dead zones appear and develop in the corners of the square cross-section. In this situation, the width of the deforming zone decreases and progressively reduces to a thin band around the central plug. Finally, the flow stops completely when the central plug simultaneously merges with the dead zones and reaches the wall.

The distance ξ_b between the center of the cross-section and the boundary of the plug is displayed on Fig. 9, as well as the distance ξ_m between the center of the square and the boundary of the dead zone. The distances are measured along the diagonal axis. The size variation of the rigid zones is similar to the one observed for a total adhesion.

The location y_m of the dead zone boundary is compared to y_T on Fig. 10, with Bi . Both curves decrease and first keep a constant distance to each other, then, in the vicinity of Bi_A , y_T quickly falls to 0, while y_m decreases to $y_m(Bi_T)$. It seems that $y_m(Bi_T) \approx y_T(0)$: along a side of the cross-section, the maximum extension of the dead zone and the minimum extension of the stick region seem to be the same. The

variations of y_m and y_T mean that adhesion occurs on a part of the wall that is larger than the part covered by the rigid zones.

As a conclusion for this case $S = 0.6$, three distinct flow regimes have been identified:

- (i) adhesion in the corner and slip at the wall for $Bi \in [0; Bi_A]$,
- (ii) adhesion everywhere for $Bi \in]Bi_A; Bi_T]$,
- (iii) blocking for $Bi > Bi_T$,

in the first two regimes, a quasi-circular central plug develops, as well as concave dead zones in the corners. All the rigid zones are separated by a deforming layer: the greater Bi , the thinner the layer.

4.2.2. Convergence to a block translation

Let us fix here $S = 0.45$ and compare the results to the previous case where S was equal to 0.6.

Let us begin with the behaviour inside the flow domain, considering Fig. 11. The velocity profiles are represented along the horizontal symmetry axis, for some Bi . As for section 4.2.1, the curves are concave, and for each x on the axis the velocity decreases for increasing Bi . Moreover, a plateau develops for $Bi > 0$ and fills the width of the domain for $Bi > Bi_C$, with $Bi_C \approx 0.5$. This corresponds to a central plug which reaches the wall for $Bi = Bi_C$. On Fig. 11.b, the velocity profiles are displayed on the diagonal axis. A plateau is developing as well, with increasing length; for increasing Bi . Let us in particular consider the velocity near the corners ($\xi = \sqrt{2}$): for $Bi = 0.2$, the velocity is 0, however when increasing Bi the velocity becomes positive. This means that dead zones may appear for small Bi but vanish when Bi increases. This leads us to the following detailed analysis of the development of the rigid zones.

On Fig. 12, a circular plug is developing when Bi increases. The plug touches the wall and goes on growing while slipping on the wall when Bi is increased. For $Bi > Bi_T \approx 0.71$, the plug fills the whole cross-section. The contact between the plug and the wall is the first main difference with the behaviour observed in section 4.2.1.

On the zoom Fig. 13, the area of the dead zones in the corners increases with Bi , as usual. However, when Bi reaches a particular value and then goes beyond, the rigid zones vanish. This is the second main difference with the section 4.2.1. In addition, another important difference is the size of the dead zones, as they remain here very small (the zoom shows the corner for $0.98 \leq y \leq 1$).

The plug velocity is given as a function of Bi on Fig. 14.a. The velocity decreases and smoothly tends to a constant value $U_T = 0.05$ at $Bi = Bi_T$. For $Bi > Bi_T$, the flow is therefore a unique rigid block translating with velocity¹ $U_T = 0.05$. This convergence to a slipping block is the third main difference with the cessation of flow case of section 4.2.1.

The flow rate is represented on Fig. 14.b, it is a decreasing function of Bi , it seems to smoothly tend to $U_T \approx 0.05$ at $Bi = Bi_T$.

In order to compare the evolution of the size of the rigid zones, two distances along the diagonal axis are represented as functions of Bi on Fig. 15: the distance ξ_b between the center and the boundary of the plug, and the distance ξ_m between the center of the square and the boundary of the dead zone. The curve² $(Bi; \xi_b(Bi))$ seems straight, this means that the plug size increases until the cessation of flow regime is reached. In the other hand, the curve $(Bi; \xi_m(Bi))$ on Fig. 15.b has a minimum at $Bi \approx 0.22$

¹ Theoretical developments about U_T are presented in appendix.

² for a real function f defined for $x \geq 0$, the notation $(x; f(x))$ is used here as a shortcut to denote the curve defined by the set of points $\{(x, f(x)); x \geq 0\}$.

because small dead zones appear, with first increasing size, but finally with decreasing size, until they vanish at $Bi \approx 0.37$.

Let us now consider the velocity profiles at the wall on Fig. 16.a. For an increasing Bi , the velocity decreases at the center while it increases near the corner. A plateau begins to grow from the center of the wall for $Bi > Bi_C$, this is because the central plug comes into contact with the wall at $Bi = Bi_C$. The part of the wall where the velocity is constant (contact region between plug and wall) becomes larger and finally is the entire wall for $Bi = Bi_T$. For $Bi \geq Bi_T$, $u = U_T \approx 0.05$, because all the fluid in the pipe is then translating as a single block at the velocity U_T .

The maximum velocity at the center of the wall, denoted $u_{max;\partial\Omega}$, is the velocity of the central plug for $Bi \geq Bi_C$, and is represented on Fig. 16.b. It regularly decreases and smoothly reaches U_T at $Bi = Bi_T$.

We can notice the existence of a number $Bi_S \approx 0.37$ beyond which the fluid slips everywhere. For $Bi < Bi_S$, a stick-slip transition point y_T can be defined. This point is an increasing function of Bi , as it can be seen on Fig. 17. The point y_T is compared to the position of the dead zone boundary y_m , on Fig. 17. The curve $(Bi; y_m(Bi))$ exhibits the non-monotonic behaviour already described for ξ_m with a minimum at $Bi \approx 0.22$ and then full slip at $Bi = Bi_S$. Both curves y_m and y_T meet at $Bi = Bi_S$, i.e. the dead zones disappear only when the slip is everywhere.

In this section, the analysis of the results can be summarised as follows:

- There exists a value $Bi_S \approx 0.37$ above which the material slips on the whole boundary, and below which the slip is partial.
- The stick region decreases with Bi until the full slip occurs at $Bi = Bi_S$.
- A central plug grows when Bi increases.
- The plug reaches the wall at $Bi = Bi_C \approx 0.5$.
- The plug fills the whole pipe when $Bi > Bi_T \approx 0.71$, then the material translates with the constant velocity $U_T \approx 0.05$.
- Small dead zones appear when Bi increases, and then vanish for $Bi < Bi_C$.

4.3. Identification of the flow regimes

In the Newtonian case [18], we have shown the existence of two numbers S_A and S_G characterising the velocity profile at the boundary of the cross-section :

- for $0 \leq S \leq S_G$, the fluid slips on all the wall,
- for $S_A \leq S$, the fluid sticks on all the wall,
- for $S_G < S < S_A$, the fluid sticks in the corners while it slips on the remainder of the wall.

The study of the role of Bi for $S \neq 0$ in the sections 4.2.1 and 4.2.2 has shown that S_A and S_G still exist for $Bi \neq 0$, leading to a block translation, possibly with a zero velocity. The synthesis Fig. 18 completes this analysis, by displaying S_A and S_G as functions of Bi , and Bi_T as a function of S . The curves delimit five flow regimes:

- (i) full adhesion (A),
- (ii) full slip (G),
- (iii) adhesion in the corners, slip elsewhere (A+G),
- (iv) cessation of flow (B),
- (v) block translation (T).

The curves $(Bi; S_A(Bi))$ and $(Bi; S_G(Bi))$ have opposite variation and join at $X = (Bi_T(S_T), S_T) \approx (0.71, 0.5)$. Then, they remain identical for $Bi \geq Bi_T(S_T)$. The number $Bi_T(S)$ only varies in $S \in [S_T; 0.53]$ from $Bi_T(S_T) = Bi_T(0) \approx 0.71$ to $Bi_T(0.53) = Bi_T(\infty) = \frac{2}{2+\sqrt{\pi}}$. Thus, for any fixed S , when Bi increases, the flow tends to:

- either a full adhesion and then a cessation of flow (for $S > S_T$), then the stop value $Bi_T(\infty)$ does not depend on S if $S - S_T$ is high enough,
- or a full slip and then a block translation (for $S < S_T$), the value $Bi_T = Bi_T(0)$ does not depend on S .

Moreover, the curve $(S; Bi_T(S))$ only varies when it is identical to $(Bi; S_A(Bi))$, for $S_T \leq S \leq S_A(Bi_T(\infty))$. Notice that we found $S_A(Bi_T(\infty)) = Bi_T(\infty)$, this means: for a given S between S_T and $Bi_T(\infty)$, when Bi increases, the slipping exists somewhere on the wall until the stopping value $Bi = Bi_T(S)$ is reached (with $Bi_T(S)$ between $Bi_T(\infty)$ and $Bi_T(0)$).

In the sections 4.2.1 and 4.2.2, two particular values of S have evidenced that the qualitative evolution of the flow with Bi depends on the sign of $S - S_T$. In the following, the investigation of the flow structures (rigid-fluid boundary, stick-slip transition) is completed with some intermediate values of S between 0.45 and 0.6 (displayed on Fig. 18).

Fig. 19.b represents the transition y_T as a function of Bi , for some S . When $S \geq S_T$, all the curves tend to 0 with a final slope close to the vertical. For intermediate values between $S = S_T = 0.5$ and $S = 0.53$, each curve increases to a maximum and then decreases to 0.

The boundaries of the rigid zones along the diagonal of the cross-section, as function of Bi , are compared on Fig. 19.a, for the values of S shown with dashed lines on Fig. 18. For a given value of Bi , the greater S the larger the rigid zones (plug and dead zones). Moreover, the phenomenon of vanishing dead zones seems to be specific to the case where $S \leq S_T$, in this case the plug grows until it fills the entire pipe at $Bi = Bi_T$. When at the contrary $S > S_T$, the dead zones grow until they meet the plug at $Bi = Bi_T$ and the flow stops.

These last observations on stick-slip transition and rigid zones evolution lead us to define three sub-regimes in the regime $A + G$:

- $AG1$: It is defined by the couples (S, Bi) from $A + G$ such that $S > S_A(Bi_T(+\infty)) \approx 0.53$. When Bi increases, full adhesion is reached (regime A).
- $AG2$: defined by the couples (S, Bi) from $A + G$ such that $1/2 = S_T \leq S \leq S_A(Bi_T(+\infty)) \approx 0.53$. When Bi increases, full adhesion and cessation of flow arise simultaneously (regime B).
- $AG3$: defined by the couples (S, Bi) from $A + G$ such that $S \leq S_T = 1/2$. When Bi increases, a full slip is reached (regime G).

All the flow configurations are summarized on Fig. 20 and Fig. 21.

5. Conclusion

This paper presents a combination of the two previous non-linear yield stress phenomena: the Poiseuille flow of a Bingham fluid with slip yield boundary condition at the wall. This problem is of practical interest, for instance for pipeline flows of yield stress fluids such as concrete and cements, and was not addressed to the best of our knowledge from a computational point of view.

An anisotropic auto-adaptive mixed finite element method for a general pipe cross-section has been developed and applied here to the case of a square cross-section. This generalizes the works previously

achieved for two particular cases: a viscoplastic fluid with no-slip at the wall, and a Newtonian fluid with the yield-force slip law. The case of a pipe with a square cross-section has been investigated in detail. The computations cover the full range of the two main dimensionless numbers and exhibit complex flow patterns.

Considering the two main parameters S and Bi of the material, the main result is the identification of five flow regimes and three sub-regimes. More precisely:

- the limiting values of Bi and S separating the regimes have been obtained;
- the evolution of the rigid zones and stick-slip transition points has been established, with respect to Bi and S in each of the eight regimes.

In particular, we have shown the existence of a regime where slipping occurs everywhere on the wall. The results concerning this regime has important consequences on the manner yield-stress fluids in pipes are considered:

- a yield-stress fluid may not be blocked in a pipe with a plug touching the wall, even with a zero shear rate in the whole pipe,
- rigid zones in corners may not exist for $Bi \neq 0$,

Another uncommon result is that dead zones in corners may reduce their area when the Bi number increases (for $S \leq S_T$).

For Bi large enough, the material is a unique rigid zone. Using variational analysis for a possibly non-square cross section, we found that the velocity of the translating block of material is: $U_T = \max(0, S_T - S)$, where $S_T = \text{area}(\Omega)/\text{length}(\partial\Omega)$. For $S > S_T$, we recover the well-known case where the fluid is blocked.

Finally, the simulations results have evidenced complex flow pattern, which have been caught thanks to the use of an auto-adaptive mesh process. The completeness of the results demonstrates the efficiency of the numerical method.

Appendix: main critical values of the dimensionless numbers

$S_A(Bi)$: for $Bi \geq 0$, adhesion at the wall for $S \geq S_A$

$S_G(Bi)$: for $Bi \geq 0$, slip at the wall for $S \leq S_G$

$Bi_A(S)$: for $S \geq S_T$, adhesion at the wall for $Bi \geq Bi_A$

$Bi_T(S)$: for $S \geq S_T$, stopped flow for $Bi \geq Bi_T$

for $S \leq S_T$, block translation for $Bi \geq Bi_T$

$Bi_S(S)$: for $S \leq S_T$, slip at the wall for $Bi \geq Bi_S$

Appendix: some theoretical results

It is possible to explain why Bi_T remains equal to $Bi_T(\infty)$ when $S > S_A$, using a result proved in [30] and [5]. In the present case, if S and Bi are so that $u_{\partial\Omega} = 0$, there exists a value Bi_T defined by:

$$Bi_T = \sup \left\{ \frac{\int_{\Omega} v \, dx}{\int_{\Omega} |\nabla v| \, dx} ; v \in H_0^1(\Omega) \text{ and } \int_{\Omega} |\nabla v| \, dx \neq 0 \right\}, \quad (40)$$

such that $u = 0$ if $Bi \geq Bi_T$, and $u > 0$ otherwise. Hence, Bi_T does not depend on S and this remains true as far as $u_{\partial\Omega} = 0$ on both side of the curve $(S; Bi_T(S))$. Moreover, the present results concerning the limit of the cessation of flow regime have a good agreement with the mathematical work of Ionescu and Sofonea [31]. The results of these authors are:

(Ionescu-Sofonea [31], theorem 4.1., page 294)

- (i) The set B is convex and (topologically) closed,
- (ii) If $(Bi, S) \in B$, then $[Bi, +\infty[\times [S, +\infty[\subset B$,
- (iii) There exists numbers L_1 and L_2 such that : $B \subset [L_1, +\infty[\times [L_2, +\infty[$.

Following the same authors, let us moreover introduce the function:

$$F_1(Bi, S) = \inf \left\{ Bi \int_{\Omega} |\nabla v| \, dx + S \int_{\partial\Omega} |\gamma v| \, ds - \int_{\Omega} v \, dx ; v \in H^1(\Omega) \text{ and } \int_{\Omega} |\nabla v|^2 \, dx + \int_{\partial\Omega} |\gamma v|^2 \, ds = 1 \right\} \quad (41)$$

The function F_1 is concave upper semi-continuous, for fixed Bi and S , $F_1(\cdot, S)$ and $F_1(Bi, \cdot)$ are increasing and the numbers L_1 and L_2 are therefore determined as follows (see [31], Lemma 2.1, page 294):

$$L_1 = \lim_{S \rightarrow +\infty} \inf \{ Bi \geq 0 ; F_1(Bi, S) \geq 0 \} \quad (42)$$

$$L_2 = \lim_{Bi \rightarrow +\infty} \inf \{ S \geq 0 ; F_1(Bi, S) \leq 0 \}$$

for instance, considering the results of the present article, it is possible to precise: $L_2 = S_T$ and, for the square cross-section, $L_1 = Bi_T(\infty) = \frac{2}{2+\sqrt{\pi}}$.

Another result characterises the blocking values of Bi as functions of S :

(Ionescu-Sofonea [31], theorem 5., page 295)

Let us define $G_1 :]0; +\infty[\rightarrow]0; +\infty[$ by :

$$G_1(S) = \sup \left\{ \frac{\int_{\Omega} v \, dx - S \int_{\partial\Omega} |\gamma v| \, ds}{\int_{\Omega} |\nabla v| \, dx} ; v \in H^1(\Omega) \text{ and } \int_{\Omega} |\nabla v| \, dx \neq 0 \right\} \quad (43)$$

for all $S \geq S_T$, the following properties are satisfied:

- (i) G_1 is a convex decreasing function,
- (ii) $Bi \geq G_1(S)$ if, and only if, $(Bi, S) \in B$.

For $S \in]S_T; +\infty[$, the number $G_1(S)$ is the critical value of Bi denoted $Bi_T(S)$ in this article.

It is possible to explicitly give the velocity along the curve $(S; Bi_T(S))$, the formula is identical to the case of a circular cross-section:

$$U_T(S) = \begin{cases} \frac{1}{2} - S & \text{if } S < S_T = \frac{1}{2} \\ 0 & \text{otherwise.} \end{cases} \quad (44)$$

This leads to the following questions: does S_T depend on the geometry ? in the translation regime (T), is the velocity constant (w.r.t. Bi) when Bi increases ? For the answer, let us consider a couple (S, Bi)

in the regime T . The velocity is constant in Ω and positive³. The variational slip law:

$$\int_{\partial\Omega} \gamma u (\zeta - \gamma u) \, ds + S \left\{ \int_{\partial\Omega} |\zeta| \, ds - \int_{\partial\Omega} |\gamma u| \, ds \right\} \geq \int_{\partial\Omega} \lambda (\zeta - \gamma u) \, ds \quad \forall \zeta \in L^2(\partial\Omega) \quad (45)$$

can then be simplified by replacing ζ by $u + \epsilon\zeta$, where $\epsilon > 0$ is a real number, and then by dividing by ϵ and finally letting ϵ tend to 0:

$$\int_{\partial\Omega} \gamma u \zeta \, ds + S \int_{\partial\Omega} \frac{\gamma u}{|\gamma u|} \zeta \, ds \geq \int_{\partial\Omega} \lambda \zeta \, ds \quad \forall \zeta \in L^2(\partial\Omega). \quad (46)$$

In, other words, u is a positive constant and:

$$u \int_{\partial\Omega} \zeta \, ds + S \int_{\partial\Omega} \zeta \, ds \geq \int_{\partial\Omega} \lambda \zeta \, ds \quad \forall \zeta \in L^2(\partial\Omega). \quad (47)$$

Now the equilibrium equation writes:

$$\int_{\Omega} \sigma \cdot \nabla v \, dx + \int_{\partial\Omega} \lambda \gamma v \, ds = \int_{\Omega} v \, dx \quad \forall v \in H^1(\Omega), \quad (48)$$

therefore, using (47) in which we choose $\zeta = v_{\partial\Omega}$, we obtain:

$$\int_{\Omega} \sigma \cdot \nabla v \, dx + (u + S) \int_{\partial\Omega} \gamma v \, ds = \int_{\Omega} v \, dx \quad \forall v \in H^1(\Omega), \quad (49)$$

in particular, for $v = u$:

$$\int_{\Omega} \sigma \cdot \nabla u \, dx + (u + S)u \, \text{length}(\partial\Omega) = u \, \text{area}(\Omega), \quad (50)$$

now, using the hypothesis $\nabla u = 0$, the velocity is obtained:

$$u = U_T(\Omega, S) = \frac{\text{area}(\Omega)}{\text{length}(\partial\Omega)} - S, \quad (51)$$

it leads to the value of S_T by considering $u = 0$ and assuming the monotonicity of u along $(S; Bi_T(S))$:

$$S_T = \frac{\text{area}(\Omega)}{\text{length}(\partial\Omega)}. \quad (52)$$

References

- [1] P. P. Mosolov and V. P. Miasnikov. Variational methods in the theory of viscous-plastic medium. *J. Mech. and Appl. Math. (P.M.M.)*, 29:468–492, 1965.
- [2] P. P. Mosolov and V. P. Miasnikov. On stagnant flow regions of a viscous-plastic medium in pipes. *J. Mech. and Appl. Math. (P.M.M.)*, 30:705–719, 1966.
- [3] P. P. Mosolov and V. P. Miasnikov. On qualitative singularities of the flow of a viscous-plastic medium in pipes. *J. Mech. and Appl. Math. (P.M.M.)*, 31:581–585, 1967.
- [4] R. R. Huilgol. A systematic procedure to determine the minimum pressure gradient required for the flow of viscoplastic fluids in pipes of symmetric cross-section. *J. non-Newton. Fluid Mech.*, 136:140–146, 2006.
- [5] G. Duvaut and J. L. Lions. *Les inéquations en mécanique et en physique*. Dunod, 1972.
- [6] M. Fortin. *Calcul numérique des écoulements des fluides de Bingham et des fluides newtoniens incompressibles par la méthode des éléments finis*. thèse, Paris VI, 1972.

³ the positivity seems obvious and can be shown by a method given in [5], where the author demonstrate that $u \geq 0$ in the case of adhesion at the wall.

- [7] M. Bercovier and M. Engelman. A finite element method for incompressible non-Newtonian flows. *J. Comp. Phys.*, 36:313–326, 1980.
- [8] A. J. Taylor and S. D. R Wilson. Conduit flow of an incompressible, yield-stress fluid. *J. of Rheol.*, 41:93–101, 1997.
- [9] M. Fortin and R. Glowinski. *The augmented Lagrangian method*. Elsevier, North-Holland, 1983.
- [10] R. R. Huilgol and M. P. Panizza. On the determination of the plug flow region in Bingham fluids through the application of variational inequalities. *J. non-Newton. Fluids Mech.*, 58:207–217, 1995.
- [11] R. R. Huilgol and Z. You. Application of the augmented lagrangian method to steady pipe flows of Bingham, Casson and Herschel-Bulkley fluids. *J. non-Newton. Fluid Mech.*, 128:126–143, 2005.
- [12] P. Saramito and N. Roquet. An adaptive finite element method for viscoplastic fluid flows in pipes. *Comput. Meth. Applied Mech. Engrg*, 190(40-41):5391–5412, 2001.
- [13] N. Roquet, R. Michel, and P. Saramito. Errors estimate for a viscoplastic fluid by using Pk finite elements and adaptive meshes. *C. R. Acad. Sci. Paris, Série I*, 331(7):563–568, 2000.
- [14] N. Roquet and P. Saramito. An adaptive finite element method for Bingham fluid flows around a cylinder. *Comput. Appl. Meth. Mech. Engrg.*, 192(31-32):3317–3341, 2003.
- [15] R. Weber and C. Van Amerongen. *The transport of concrete by pipeline*. C. and C. A. library translation, no. 129, London: Cement and Concrete Association, 1969.
- [16] D. Kaplan, F. de Larrard, and T. Sedran. Design of concrete pumping circuit. *ACI Mater. J.*, 102(2):110–117, 2005.
- [17] A. Fortin, D. Côté, and P. A. Tanguy. On the imposition of friction boundary conditions for the numerical simulation of Bingham fluid flows. *Comput. Meth. Applied Mech. Engrg.*, 88:97–109, 1991.
- [18] N. Roquet and P. Saramito. Stick-slip transition capturing by using an adaptive finite element method. *Mathematical Modelling and Numerical Analysis*, 38(2):249–260, 2004.
- [19] E. C. Bingham. *Fluidity and Plasticity*. McGraw-Hill, New York, 1922.
- [20] J. G. Oldroyd. A rational formulation of the equations of plastic flow for a Bingham solid. *Proc. Camb. Phil. Soc.*, 43:100–105, 1947.
- [21] I. R. Ionescu and B. Vernescu. A numerical method for a viscoplastic problem. An application to the wire drawing. *Int. J. Engrg. Sci.*, 26:627–633, 1988.
- [22] J. Haslinger, I. Hlaváček, and J. Nečas. *Numerical methods for unilateral problems in solid mechanics*. Handbook of Numerical Analysis, vol. IV, P. G. Ciarlet and J. L. Lions (ed.), 1996.
- [23] N. Kikuchi and J. T. Oden. *Contact problems in elasticity: A study of variational inequalities and finite element methods*. SIAM Studies in Applied Mathematics, 1988.
- [24] R. A. Adams. *Sobolev spaces*. Academic Press, 1975.
- [25] R. Glowinski, J. L. Lions, and R. Trémolières. *Numerical analysis of variational inequalities*. North Holland, Amsterdam, 1981.
- [26] H. Borouchaki, P. L. George, F. Hecht, P. Laug, and E. Saltel. Delaunay mesh generation governed by metric specifications. Part I : Algorithms. *Finite Elem. Anal. Des.*, 25:61–83, 1997.
- [27] F. Hecht. *Bidimensional anisotropic mesh generator*. INRIA, 1997. <http://pauillac.inria.fr/cdrom/www/bamg/eng.htm>.
- [28] P. Saramito, N. Roquet, and J. Étienne. Rheolef home page. <http://www-lmc.imag.fr/lmc-edp/Pierre.Saramito/rheolef/>, 2006.
- [29] P. Saramito, N. Roquet, and J. Étienne. Rheolef users manual. Technical report, LMC-IMAG, 2006. <http://www-lmc.imag.fr/lmc-edp/Pierre.Saramito/rheolef/usrman.ps.gz>.
- [30] R. Glowinski. *Numerical methods for non-linear variational problems*. Springer-Verlag, 1980.
- [31] I. R. Ionescu and M. Sofonea. The blocking Property in the study of the Bingham fluid. *Int. J. Engrg. Sci.*, 24:289–297, 1986.

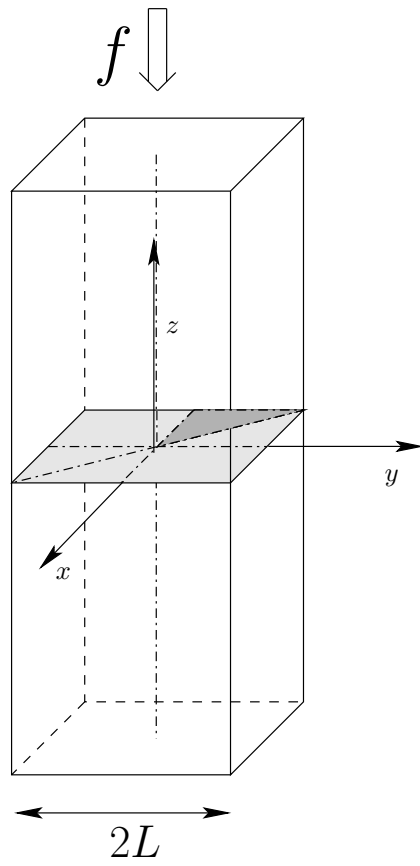


Figure 1. Square tube cross-section: three dimensional view

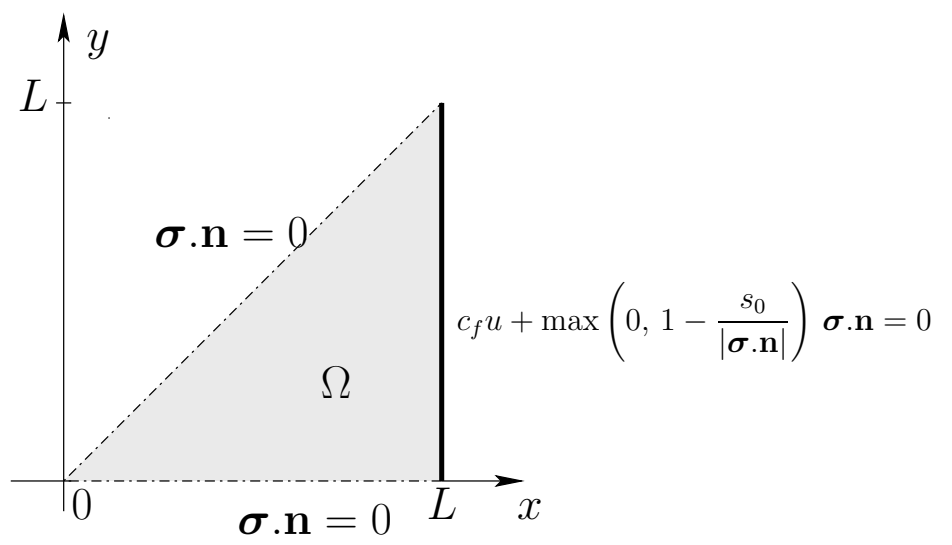


Figure 2. The domain of computation Ω and the boundary conditions.

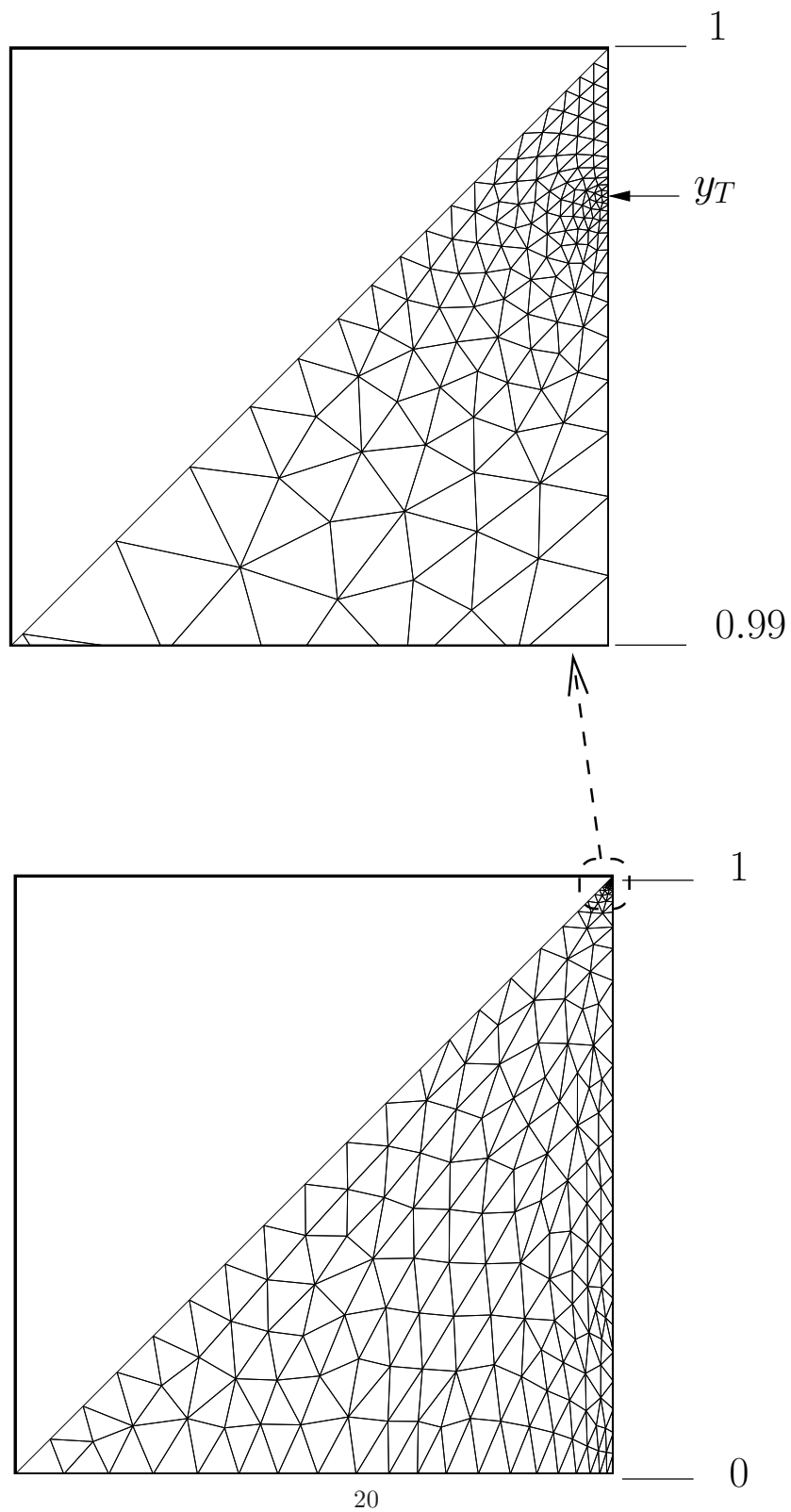


Figure 3. Zoom $\times 100$ at the neighborhood of the stick-slip transition point: after 15 mesh adaptation iterations ($Bi = 0$, $S = 0.385$).

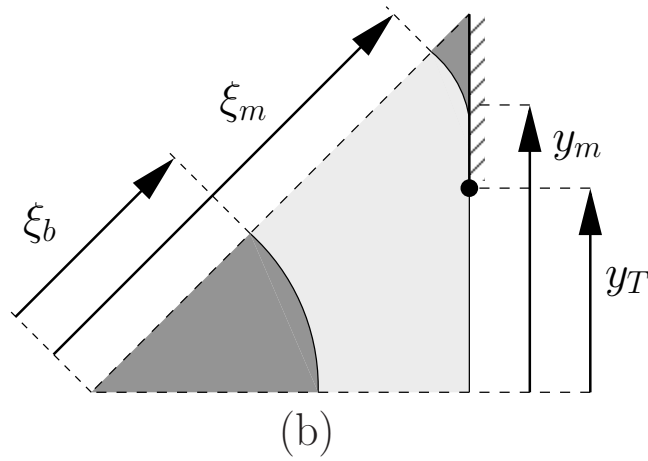
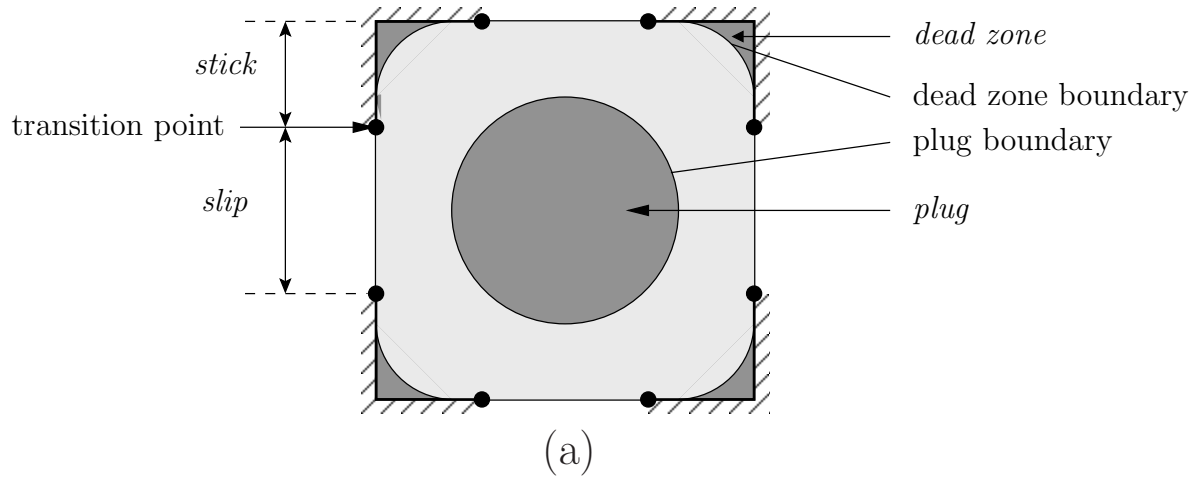
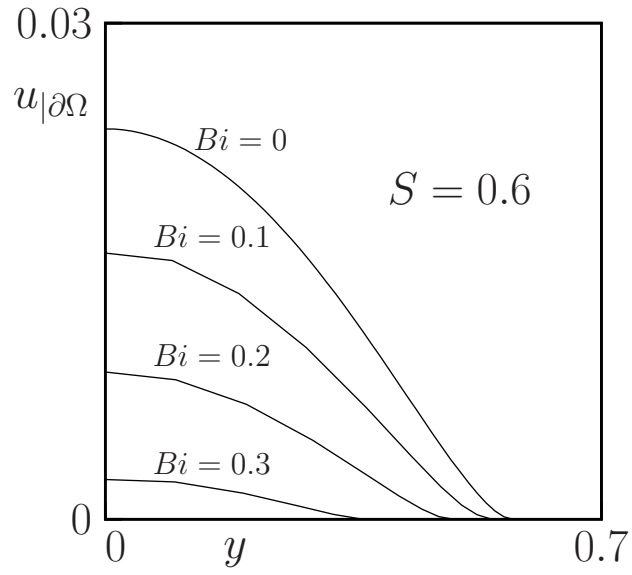
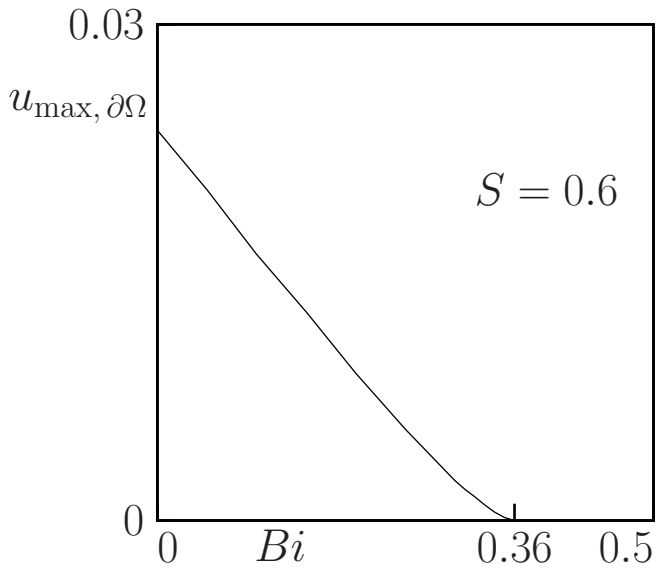


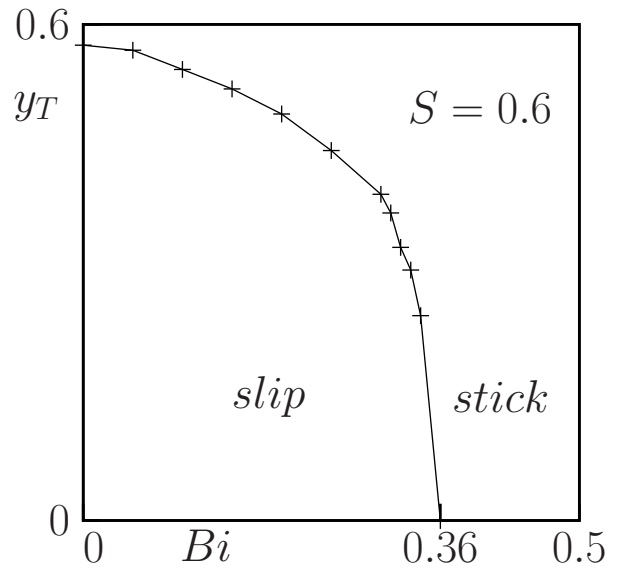
Figure 4. Schematic view of the cross-section: (a) the typical patterns of the flow; (b) some quantities relevant for the analysis.



(a)



(b)



(c)

Figure 5. Velocity at the wall for $S = 0.6$: (a) dependence upon Bi ; (b) intersection with the y -axis: maximum wall velocity versus Bi ; (c) intersection with the x -axis: coordinate y_T of the stick-slip transition point as a function of Bi .

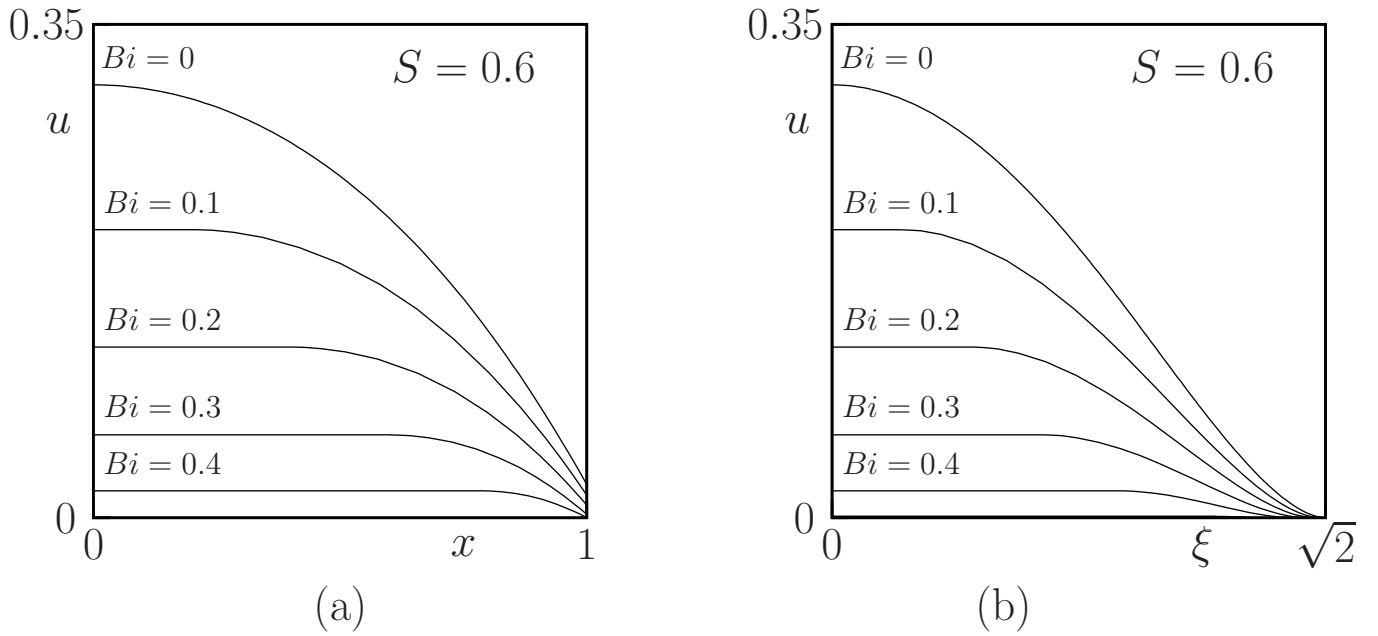


Figure 6. Velocity profiles for different values of Bi and $S = 0.6$: (a) cut along the horizontal axis $y = 0$; (b) cut along the diagonal $y = x$.

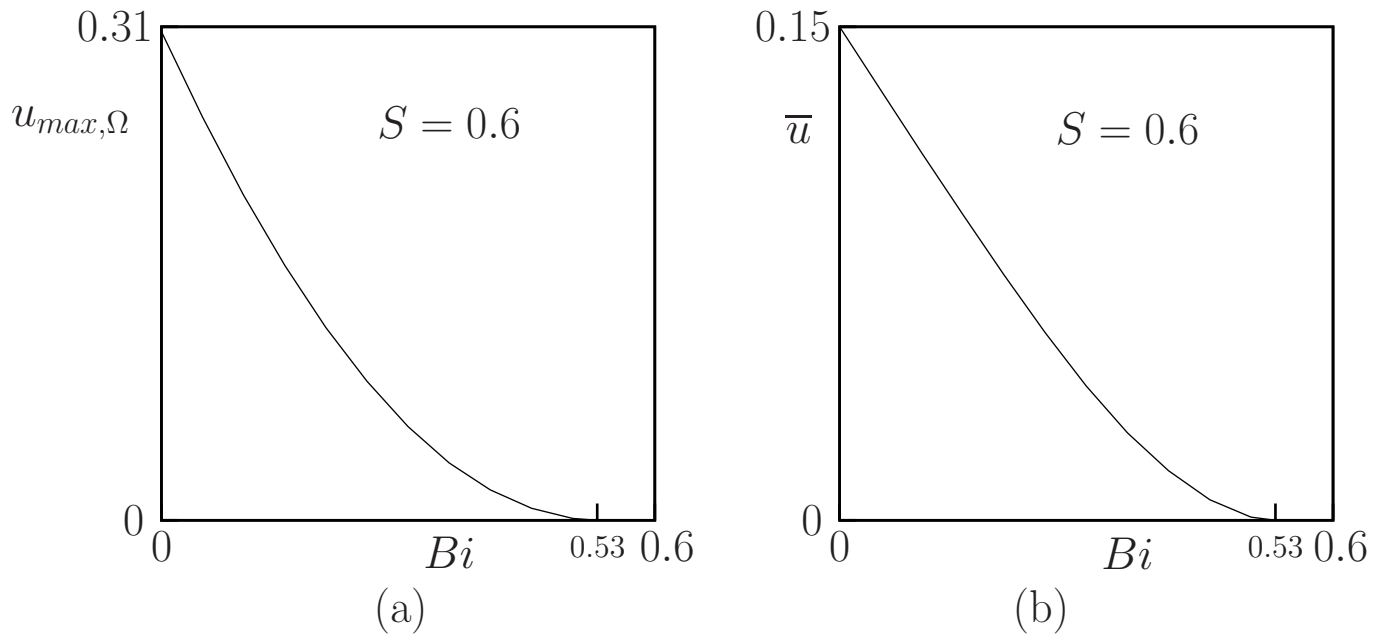


Figure 7. (a) Maximum velocity $u_{max,\Omega}$ versus Bi for $S = 0.6$; (b) Flow rate \bar{u} versus Bi for $S = 0.6$.

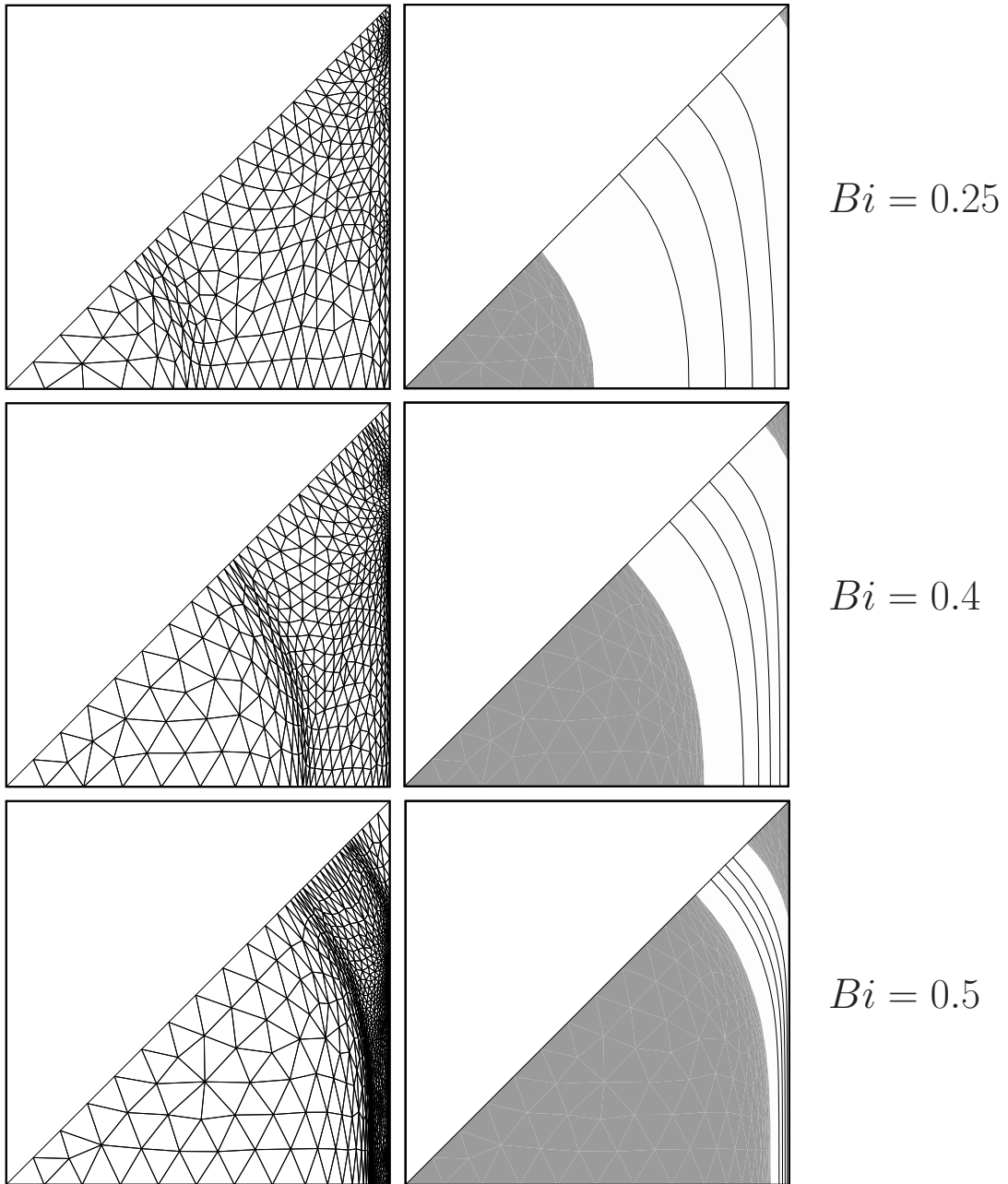


Figure 8. Adapted meshes and their associated solutions for $S = 0.6$: rigid zones in dark gray, deforming zones in light gray, and isovalues of the velocity.

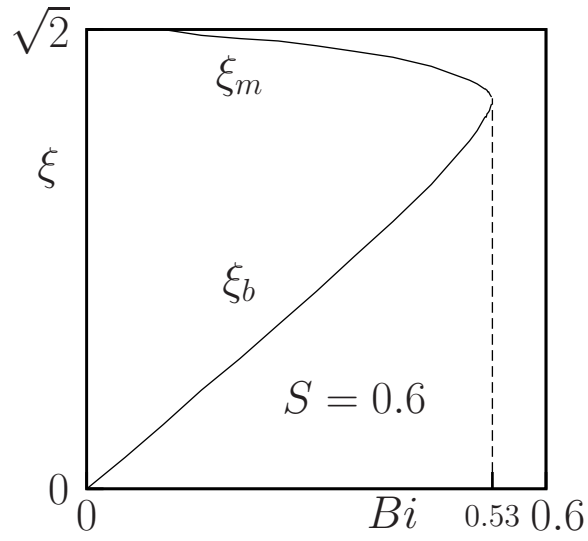


Figure 9. Position on the square diagonal of the dead zone boundary ξ_m and the plug boundary ξ_b , as functions of Bi , with $S = 0.6$.

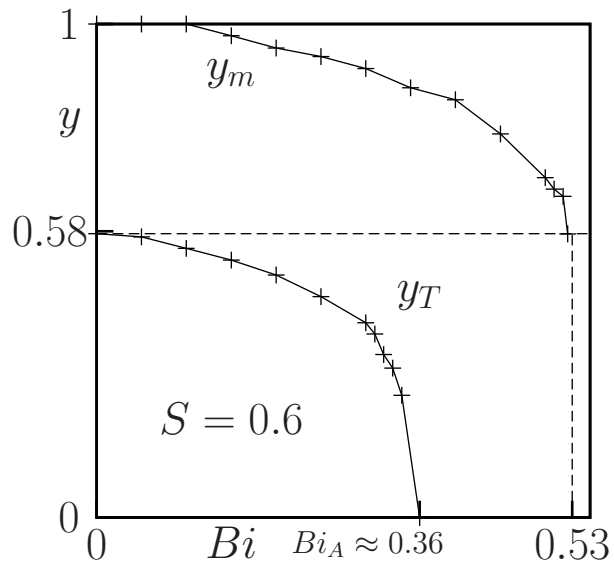


Figure 10. Positions on the wall of the free boundaries, as functions of Bi , with $S = 0.6$: position y_T of the stick-slip transition point, position y_m of the dead zone boundary.

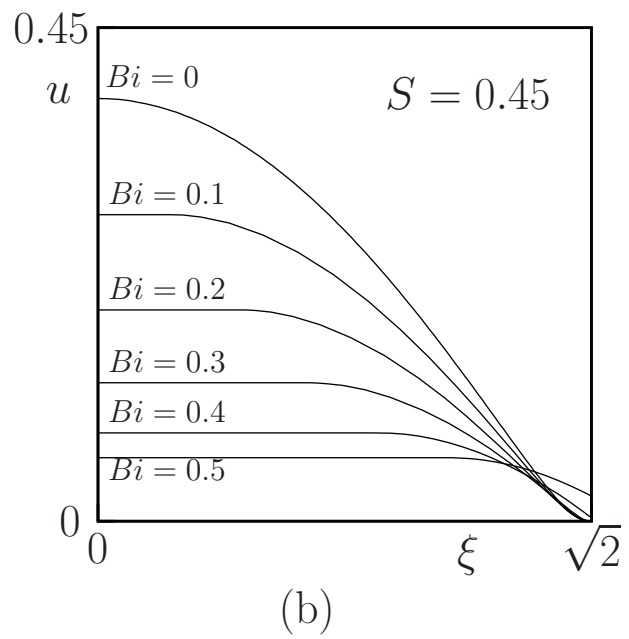
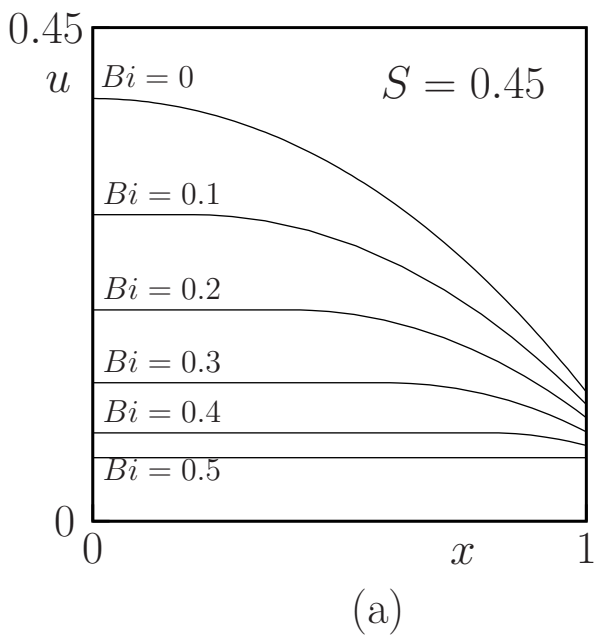


Figure 11. Velocity profiles for some values of Bi and $S = 0.45$: (a) cut along the horizontal axis ; (b) cut along the diagonal.

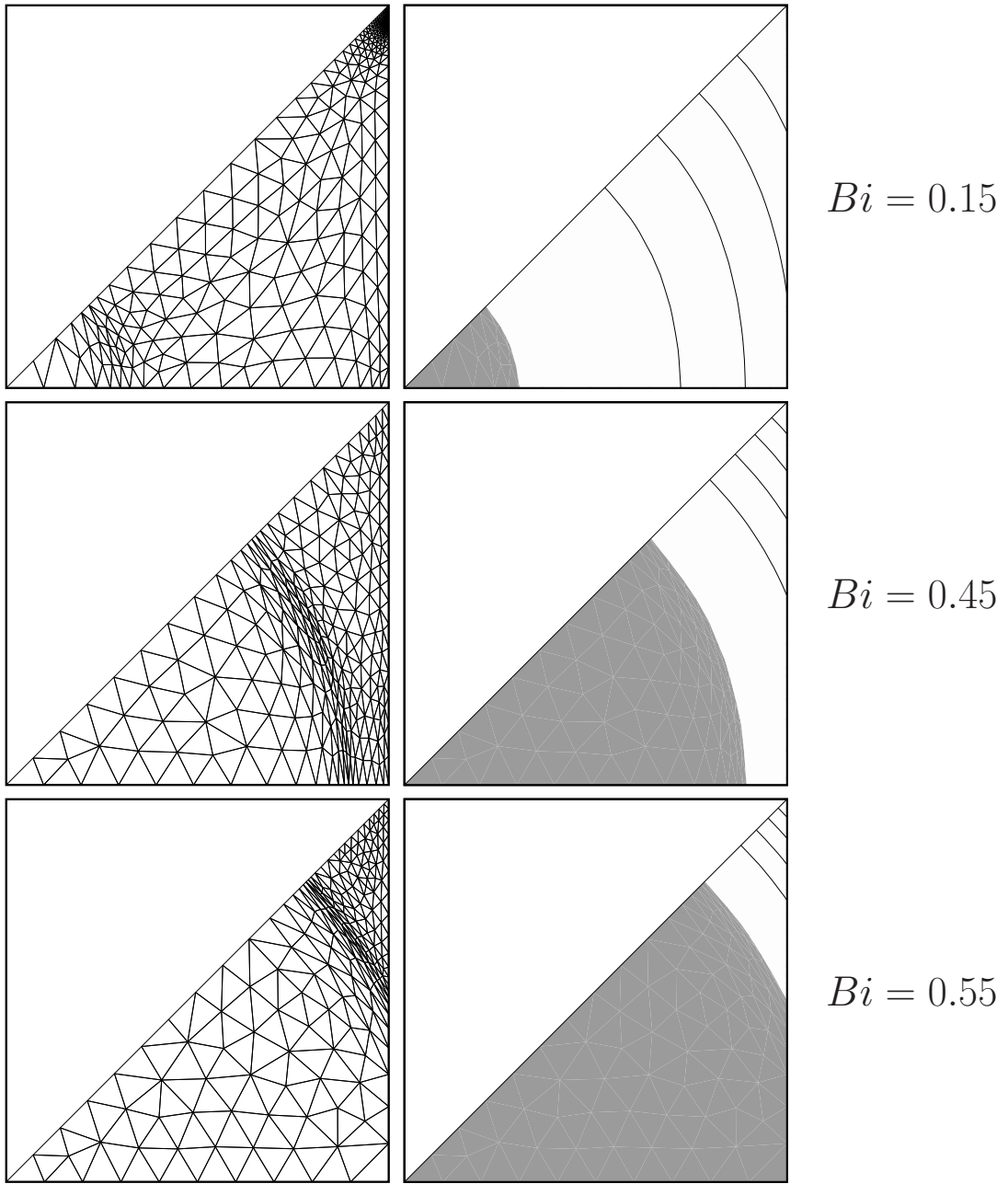


Figure 12. Adapted meshes and associated solutions for $S = 0.45$: rigid zones in dark gray, deforming zones in light gray, and isovalues of the velocity.

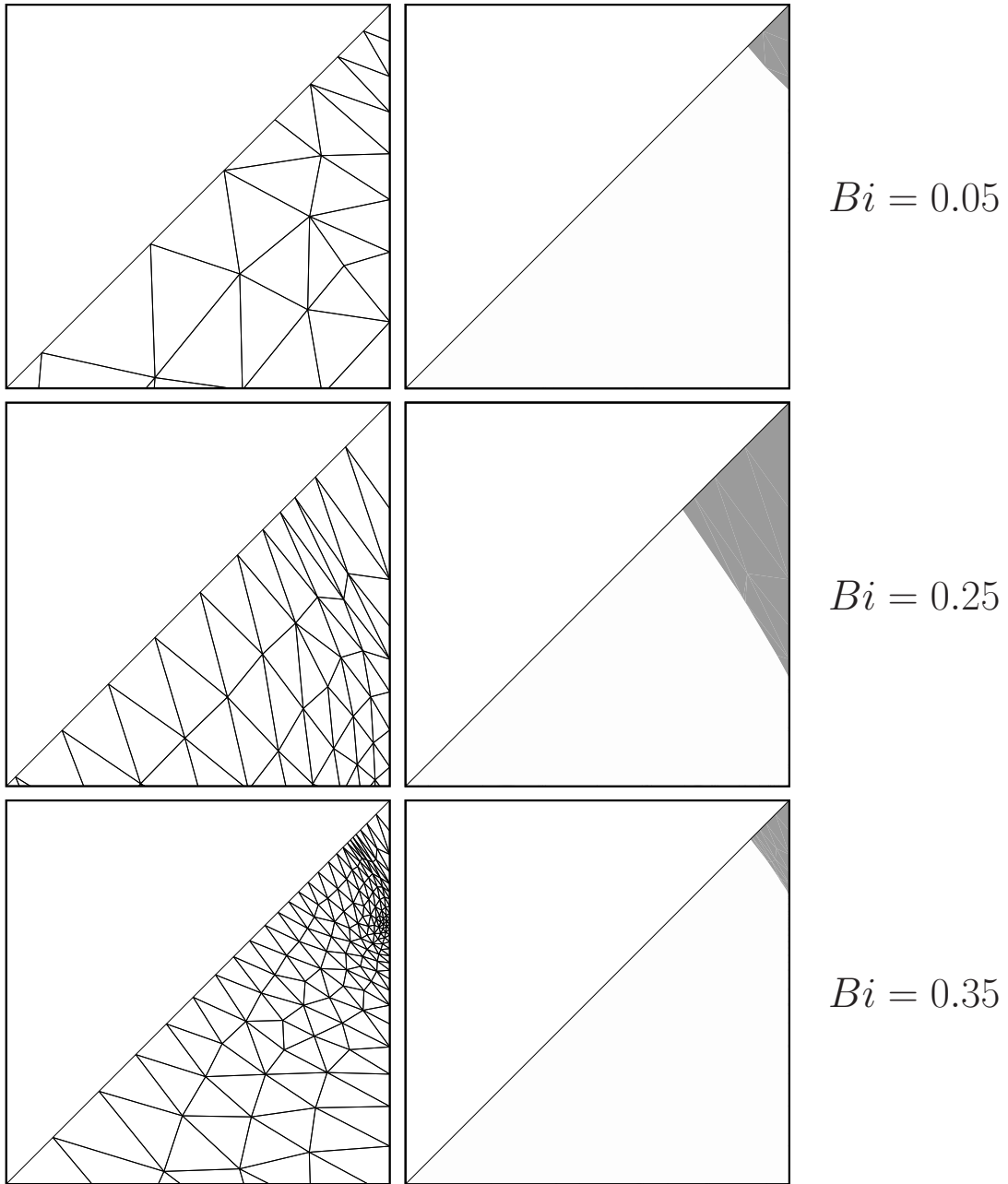


Figure 13. Adapted meshes and associated solutions, zoomed in the corner ($0.98 \leq y \leq 1$) for $S = 0.45$: rigid zones in dark gray, deforming zones in light gray.

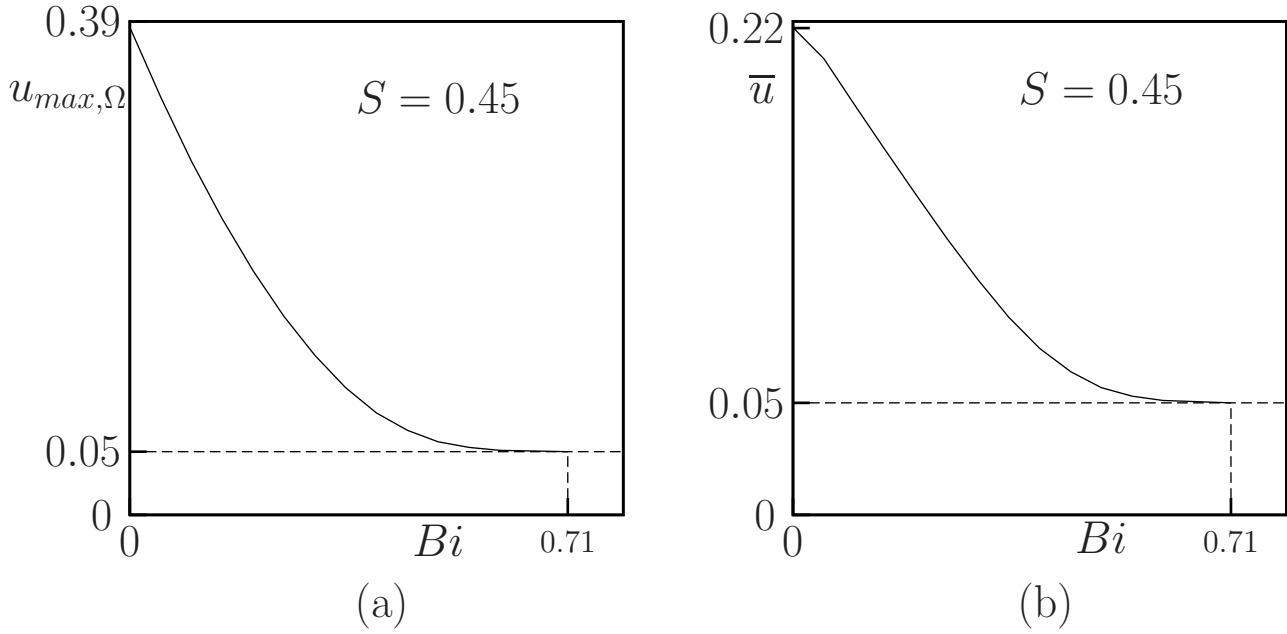


Figure 14. (a) Maximum velocity $u_{max,\Omega}$ versus Bi for $S = 0.45$. (b) Flow rate \bar{u} versus Bi , for $S = 0.45$.

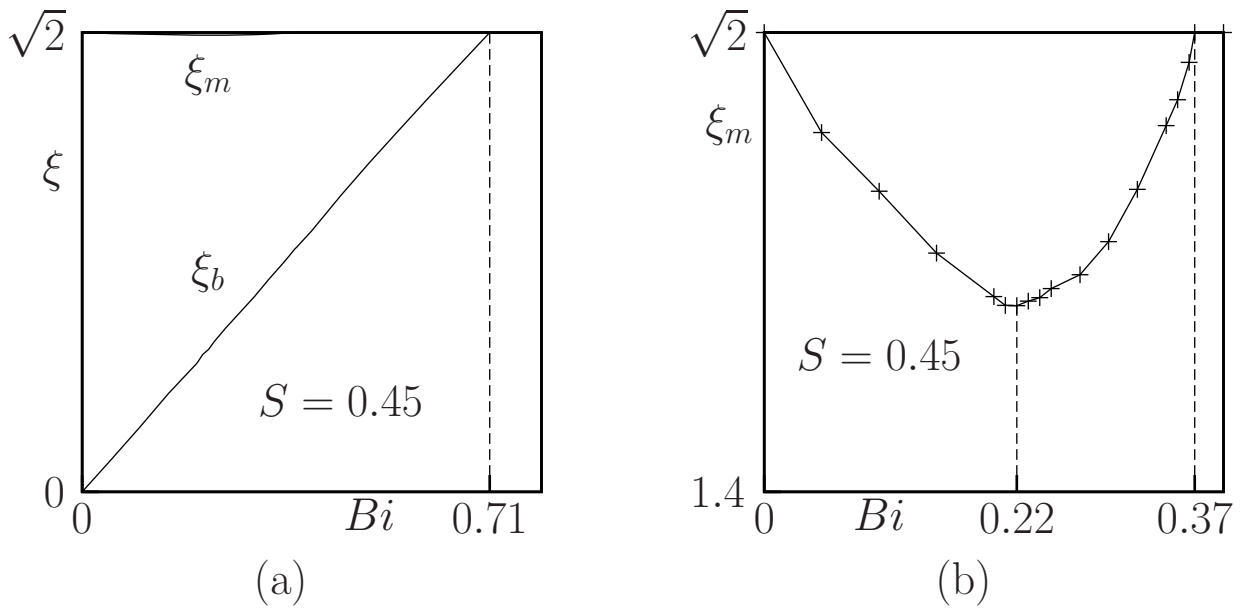


Figure 15. Position on the square diagonal of the rigid zones boundaries as functions of Bi , for $S = 0.45$: position ξ_m for the dead zones and ξ_b for the plug: (a) curves $(Bi; \xi_m(Bi))$ and $(Bi; \xi_b(Bi))$; (b) zoom on the curve $(Bi; \xi_m(Bi))$.

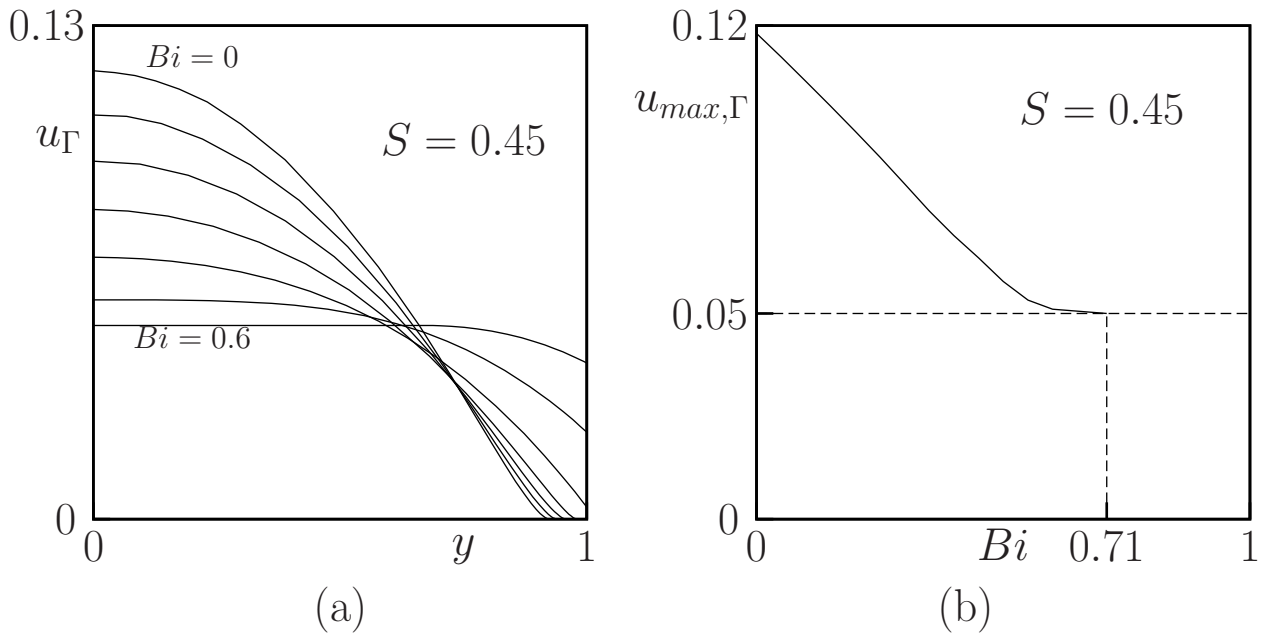


Figure 16. Velocity at the wall for $S = 0.45$ (mixed regime where both stick and slip exist): (a) for $Bi \in \{0; 0.1; 0.2; 0.3; 0.4; 0.5; 0.6\}$; (b) maximum value versus Bi .

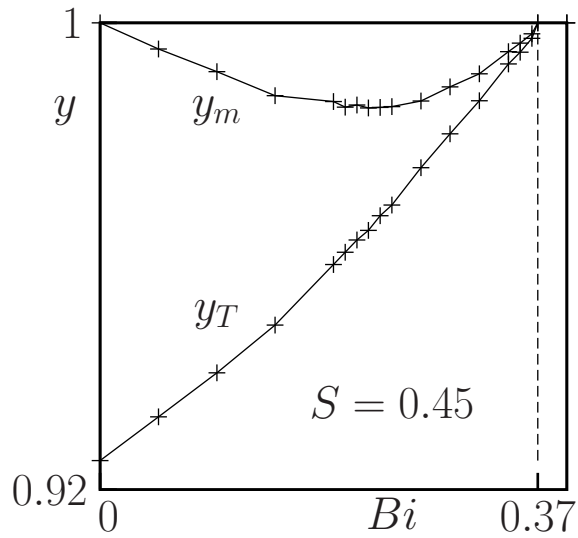


Figure 17. Position at the wall of the free boundaries as functions of Bi for $S = 0.45$: position y_m of the dead zone boundary, position y_T of the stick-slip transition.

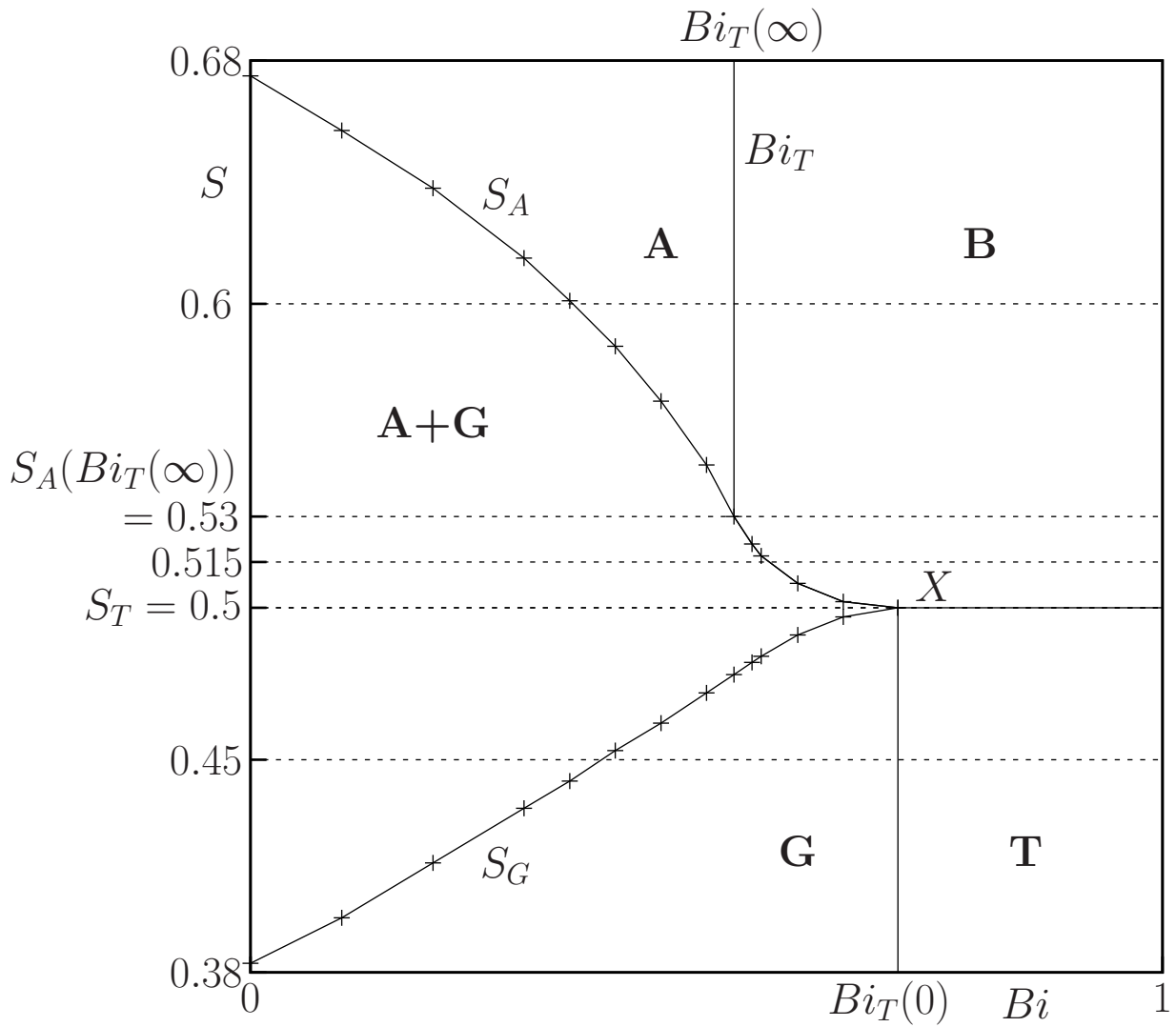


Figure 18. The main flow regimes for a square section: curves $(Bi; S_A(Bi))$, $(Bi; S_G(Bi))$ and $(Bi_T(S); S)$, and value S_T separating the regimes; particular point X and values $Bi_T(0)$, $Bi_T(\infty)$ and $S_A(Bi_T(\infty))$; representation in dashed lines of the values of S used to study the dependence of the flow upon Bi .

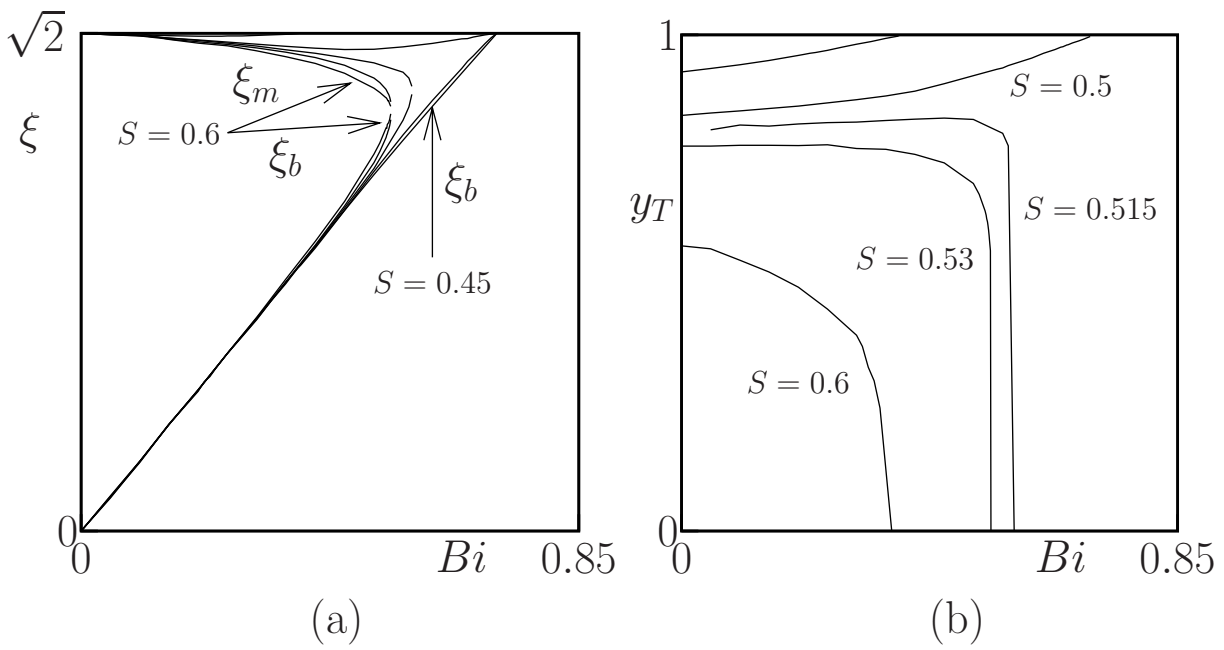


Figure 19. Evolution of the free boundaries versus Bi , for some values of S : (a) positions ξ_m of the dead zone and ξ_b of the plug along the square diagonal ; (b) position y_T of the stick-slip transition point.

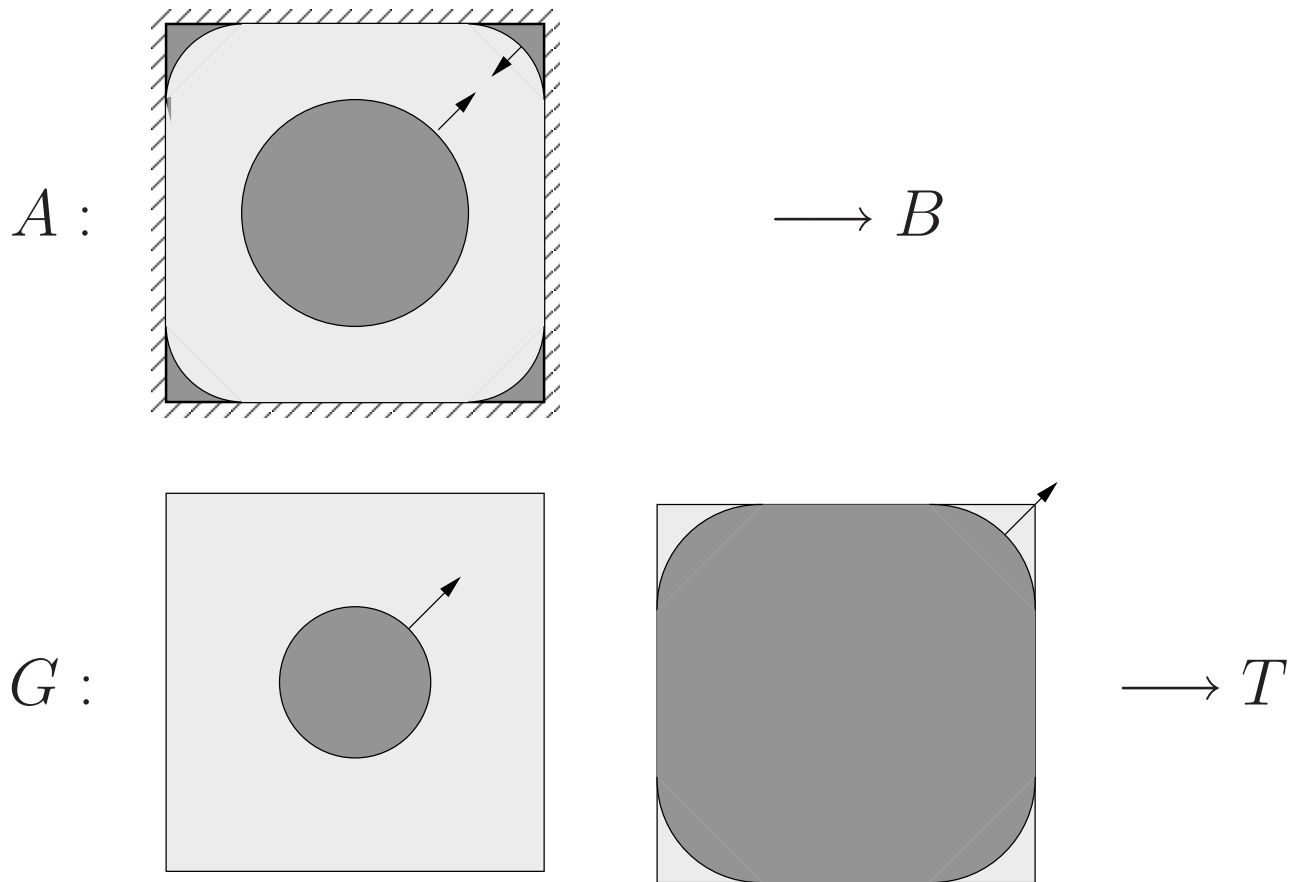


Figure 20. Schematic representation of the flow in the regimes A and G when Bi increases: evolution of the rigid zones boundaries and of the stick-slip transition points.

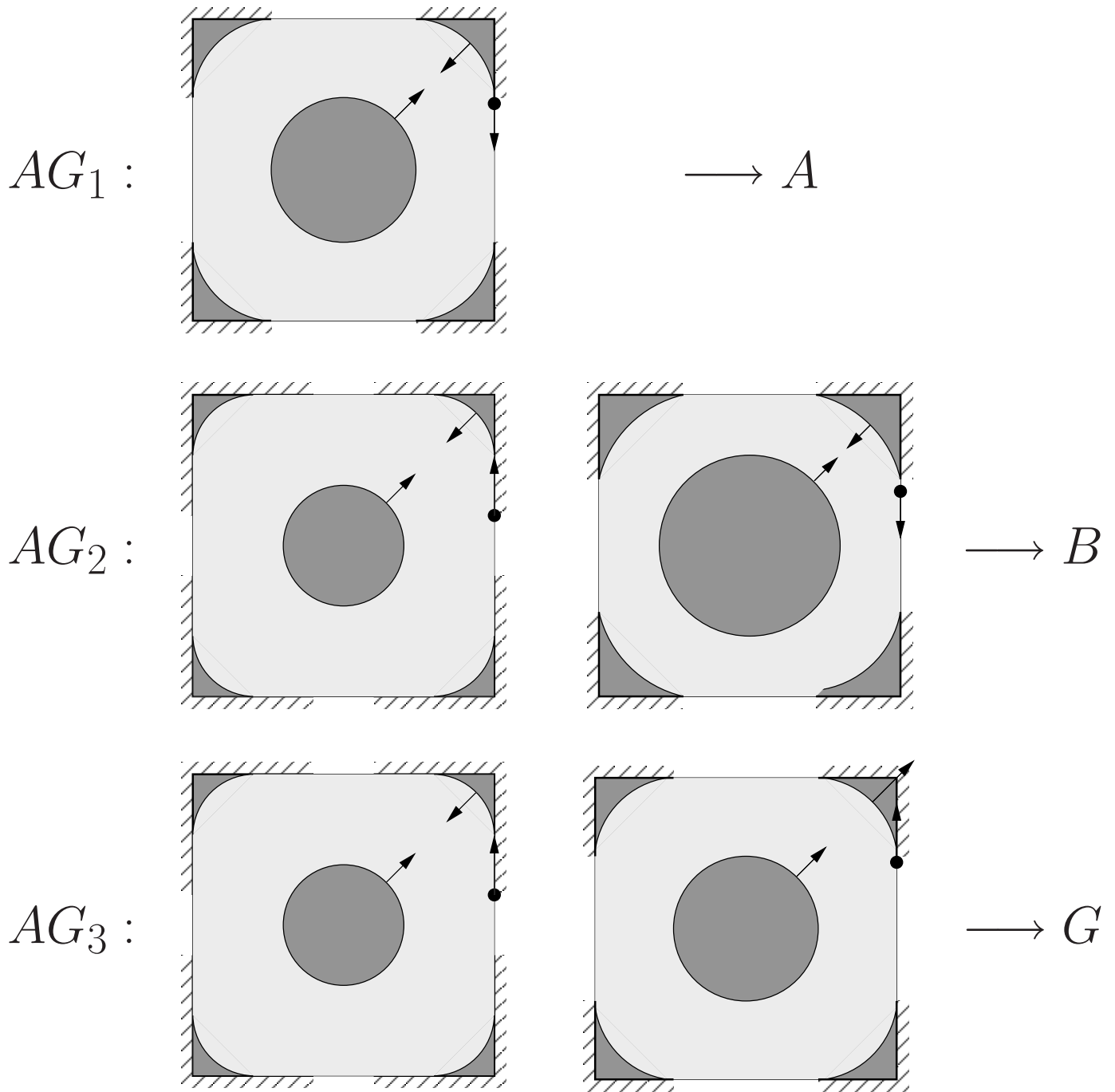


Figure 21. Schematic representation of the flow in the sub-regimes AG_1 , AG_2 and AG_3 when Bi increases: evolution of the rigid zones boundaries and of the stick-slip transition points.